NOTICE

AVIS

The quality of this microform is heavily dependent upon the quality of the original thesis submitted for microfilming. Every effort has been made to ensure the highest quality of reproduction possible.

La qualité de cette microforme dépend grandement de la qualité de la thèse soumise au microfilmage. Nous avons tout fait pour assurer une qualité supérieure de reproduction.

If pages are missing, contact the university which granted the degree.

S'il manque des pages, veuillez communiquer avec l'université qui a conféré le grade.

Some pages may have indistinct print especially if the original pages were typed with a poor typewriter ribbon or if the university sent us an inferior photocopy.

La qualité d'impression de certaines pages peut laisser à désirer, surtout si les pages originales ont été dactylographiées à l'aide d'un ruban usé ou si l'université nous a fait parvenir une photocopie de qualité inférieure.

Reproduction in full or in part of this microform is governed by the Canadian Copyright Act, R.S.C. 1970, c. C-30, and subsequent amendments.

La reproduction, même partielle, de cette microforme est soumise à la Loi canadienne sur le droit d'auteur, SRC 1970, c. C-30, et ses amendements subséquents.

Canada

Hot Deformation Behaviour of Al_2O_3/7075 Al Composites

and Their Matrix Alloy

Qin Qi

A Thesis

in

The Department

of

Mechanical Engineering

Presented in Partial Fulfilment of the Requirements

for the Degree of Master of Applied Science at

Concordia University

Montreal, Quebec, Canada

March, 1995

THE AUTHOR HAS GRANTED AN
IRREVOCABLE NON-EXCLUSIVE
LICENCE ALLOWING THE NATIONAL
LIBRARY OF CANADA TO
REPRODUCE, LOAN, DISTRIBUTE OR
SELL COPIES OF HIS/HER THESIS BY
ANY MEANS AND IN ANY FORM OR
FORMAT, MAKING THIS THESIS
AVAILABLE TO INTERESTED
PERSONS.

L'AUTEUR A ACCORDE UNE LICENCE
IRREVOCABLE ET NON EXCLUSIVE
PERMETTANT A LA BIBLIOTHEQUE
NATIONALE DU CANADA DE
REPRODUIRE, PRETER, DISTRIBUER
OU VENDRE DES COPIES DE SA
THESE DE QUELQUE MANIERE ET
SOUS QUELQUE FORME QUE CE SOIT
POUR METTRE DES EXEMPLAIRES DE
CETTE THESE A LA DISPOSITION DES
PERSONNE INTERESSEES.

THE AUTHOR RETAINS OWNERSHIP
OF THE COPYRIGHT IN HIS/HER
THESIS. NEITHER THE THESIS NOR
SUBSTANTIAL EXTRACTS FROM IT
MAY BE PRINTED OR OTHERWISE
REPRODUCED WITHOUT HIS/HER
PERMISSION.

L'AUTEUR CONSERVE LA PROPRIETE
DU DROIT D'AUTEUR QUI PROTEGE
SA THESE. NI LA THESE NI DES
EXTRAITS SUBSTANTIELS DE CELLE-
CI NE DOIVENT ETRE IMPRIMES OU
AUTREMENT REPRODUITS SANS SON
AUTORISATION.

ISBN 0-612-01357-X

Canadä

Hot Deformation Behaviour of $Al_2O_3/7075$ Al Composites

and Their Matrix Alloy

Qin Qi

ABSTRACT

Isothermal hot torsion tests were performed on two aluminum matrix composites (10% Al_2O_3/7075 Al and 15% Al_2O_3/7075 Al) and their matrix alloy(7075 Al alloy) The composites and matrix alloy were tested over the temperature range 250 to 540°C and strain rate range 0.1 to 4.0 s^{-1}. The dependence of flow stress σ and ductility on strain rate $\dot{\varepsilon}$ and temperature T is compared for the composites and matrix alloy. The flow stress decreases monotonically with increasing deformation temperature for the composites and matrix alloy, following the same relationship as the published data Flow stresses for the composites rise more rapidly than the matrix alloy and for 15% Al_2O_3/7075 Al are generally higher than for 10% Al_2O_3/7075 Al, but the difference is quite small at higher temperature The plots of log $\dot{\varepsilon}$ versus log sinh $\alpha\sigma_p$ and of log sinh $\alpha\sigma_p$ versus 1/T are approximately linear over the range of strain rate tested. Data analysis shows that activation energies (Q_{hw}) for composites are higher than that of matrix alloy and that for 15% Al_2O_3/7075 Al is higher than that for the 10% Al_2O_3/7075 Al. While the stress decreased monotonically with rising temperature and declining strain rate, the ductility for composites went through a maximum at 400°C.

ACKNOWLEDGMENTS

TABLE OF CONTENTS

LIST OF FIGURES

through the Z parameter using different α values for 7075 Al matrix:

(a) α =0.01 MPa^{-1}, (b) α =0.02 MPa^{-1}, (c) α =0.04 MPa^{-1},

LIST OF TABLES

NOMENCLATURE

A: Material Constant [s^{-1}]

L_0:   Specimen Gauge Length [mm]

m: Strain Rate Sensitivity Exponent

N: Number of Turns

n: Stress Exponent, sinh equation

n':   Stress Exponent, power law

n":   Strain Hardening Exponent

Q_c: Activation Energy for Creep [kJ/mol]

Q_{HW}:   Activation Energy for Hot Working [kJ/mol]

R: Universal Gas Constant [8.314 J/mol-K]

r: Specimen Gauge Radius [mm]

Z: Zener-Hollomon Parameter [s^{-1}]

α: Stress Multiplier [MPa^{-1}]

ε: Equivalent Strain

$\dot{\varepsilon}$:   Strain Rate [s^{-1}]

ε_f: Fracture Strain

θ: Angle of Twist per Unit Length

$\dot{\theta}$:   Rate of Twist

σ: Equivalent Flow Stress [MPa]

σ_p: Peak Flow Stress [MPa]

1. INTRODUCTION

The objective of this research is to determine the hot working behavior of two alumina particle(Al_2O_3) reinforced aluminum-matrix composites(Al_2O_3/7075 Al) and their matrix alloy(7075 Al alloy) under continuous deformation conditions at typical hot working temperatures and strain rates. Torsion testing has been established as a convenient laboratory method of studying the flow characteristics of materials during hot working. This method was employed becase it has the advantage compared to tension and compression in that a large strain can be applied to a specimen at a relatively constant rate Hot torsion testing has been used widely to simulate hot rolling schedules in order to provide optimization.

The project involves the determination of stress-strain curves and fracture strains at representative hot working temperatures and strain rates General characteristics of aluminum matrix composite and aluminum matrix alloy will be discussed in Chapter 2 The literature which describes the general hot working characteristics of the above materials then follows in Chapter 3. A description of the hot torsion machine along with its operating procedure are presented in Chapter 4. In addition, a full description of the experimental procedures adopted in the present study is also given. Chapter 4 details all experimental results and a discussion of the results follows in Chapter 6 Finally, all relevant conclusions which are drawn concerning the hot deformation characteristics of the materials based on the present work are listed in Chapter 7.

2. GENERAL MATERIAL CHARACTERISTICS

2.1 Aluminum Matrix Composites

Metal Matrix Composites (MMCs) have the advantage of attaining property combinations that are useful in service. In comparison to their base metal counterparts, MMCs are capable of increased strength, stiffness, thermal conductivity, decreased weight, improved wear resistance, higher-temperature operating limits and higher elastic modulus. In MMCs, the metal acts as the matrix, and its main function is to transfer and distribute the load to the reinforcements such as particles or fibers. This transfer of load depends on the interface bonding between the matrix and the reinforcement. The reinforced fibers or particles used in MMCs application have high yield strength and high Young's modules compared to the matrices used in a relatively ductile, low yield strength matrix such as aluminum.

Most of the commercial work on MMCs has focused on aluminum as the matrix metal (AMC) because it possesses a wide variety of properties such as good corrosion resistance, low density and medium strength. The melting point of aluminum is high enough to satisfy many application requirements, yet low enough to render composite processing reasonably convenient. The microstructures of various aluminum matrix MMCs are shown in Figure 2.1[1]. Among the many ceramic reinforcements considered for making AMC, SiC and Al_2O_3 have been found to have excellent compatibility with the aluminum matrix[2,3]. In a recent study, particulate alumina is used to manufacture
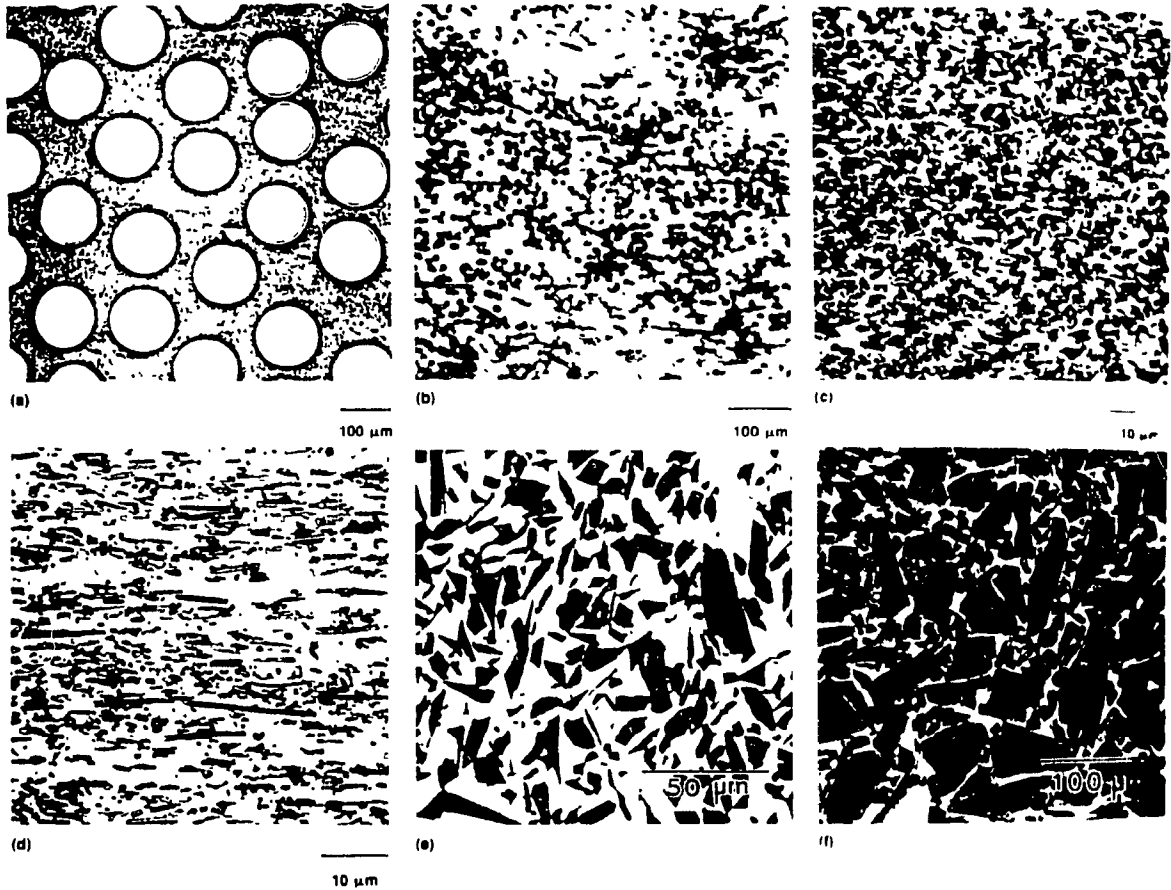
Figure 2.1   Cross section of typical fiber-reinforced MMCs. (a) Continuous-
fiber-reinforced boron/aluminum composite. (b) Discontinuous
graphite/aluminum composite. (c) A6061 aluminum alloy matrix
reinforced with 40 vol% SiC particles. (d) Whisker-reinforced
(20% vol% SiC)aluminum MMCs. (e) An Al$_2$O$_3$-reinforced (60
vol%) aluminum MMCs. (f) A highly reinforced (81 vol%) MMCs
consisting of SiC particles in an aluminum alloy matrix[1].

AMC materials through the powder metallurgy route which involves mixing, blending, pressing and sintering of the constituent powders. Particulate reinforced aluminum matrix composites have high potential for development. Like monolithic metals, particulate reinforced AMC are approximately isotropic. They can be shaped by standard metallurgical processes such as forging, rolling and extrusion[3]. Due to this ease of formability and relatively modest cost, particulate reinforced AMC have been made for use in various automotive applications. The most economical mode of producing AMC with SiC or Al_2O_3 particles is liquid metal mixing followed by DC casting into slabs and billets[4-7]. Further fabrication is conducted by traditional mechanical shaping operations both at high and ambient temperatures T[5, 7-9]. As for traditional alloys, hot working is expected to permit lower forces and greater shape change as a result of reduction in both matrix rupture and particle decohesion or cracking under reduced flow stress[7-9, 10-21] The improved matrix malleability stems from dynamic recovery (DRV); however, it is also possible that particle stimulated nucleation (PSN) of dynamic recrystallization (DRX) makes a substantial contribution[7, 8, 14, 17, 18, 21-23]. Avoidance of microcracks at particles is very important for sound products.

2.1.1 Composite System

Aluminum-matrix composites are not a single material but a family of materials whose stiffness, strength, density, thermal and electrical properties can be adjusted for specific applications[24,25]. The matrix alloy and the type, size, volume fraction and location of the reinforcement are chosen to match desired properties[26]. In general, the

ductility and fracture toughness are controlled by the matrix alloy composition and heat treatment while the stiffness and strength are determined by the reinforcement material and volume fraction. For economic reasons, high volume applications for MMCs are restricted to particle reinforced composites prepared via a liquid metallurgy or low cost powder metallurgy route. A common problem with MMCs is excessive reaction between the matrix and reinforcement, which often results in inferior properties in the composite compared with the matrix alloy. Some interfacial reaction is required, however, to achieve wetting of the particles by the melt which, in turn, is necessary to disperse the particles uniformly in the melt. In a composite system, the best properties are obtained when the reinforcement and the matrix alloy are as chemically compatible as possible[27]. The selection of the matrix alloy is based on the characteristics desired in the final product The 6xxx series alloys are widely used because of their high formabili y and overall good mechanical properties. The 7xxx series alloy are selected where strength is required

2.1.1.1 SiC Reinforcement

Much work have been carried out with different types of SiC reinforcement It is well know that SiC is thermodynamically unstable in molten Al and reacts to form Al_4C_3 and Si according to the reaction:

$$4Al + 3SiC = Al_4C_3 + 3Si \qquad\qquad (2 1)$$

The Al_4C_3 forms at the interface while the Si dissolves in the Al matrix (Figure 2 2)[28] The formation of Al_4C_3 generally leads to degradation of the mechanical properties of the reinforcement and the composite[29]. Hence this reaction should be avoided.

The effects of several modifications to SiC on the interface reaction have examined, including: Modification to the surface chemistry,Variation in particle size and Variation in SiC purity level.

(a) Modification to the surface chemistry: Silicon carbid particles usually have a vitreous surface layer of SiO_2. Therefore, the initial interfacial reaction is between SiO_2 and Al and , hence, a thick surface layer of SiO_2 can serve as a barrier for the undesirable reaction between SiC and Al. The SiO_2 layer on SiC can easily be thickened by heating in air. Figure 2.3 shows the results of X-ray Photoelectron Spectroscopy(XPS) carried out on SiC heated at 700°C and 1200°C for 60 minutes. The surface analysis of as-received SiC and of as-received SiC rinsed in 1M HF is also given in Figure 2.3 for comparison. It is estimated that heating in air at 700°C for 1 hour, increases the thickness of the oxide layer to between 30 and 50nm from the native thickness of between 2 and 4nm. The oxide layer remains vitreous up to a temperature of about 1300°C beyond which crystallisation occurs[30]. As predicted, the use of SiC preheated at 700°C in air was found to reduce the reaction between Al and SiC.

(b) Variation in particle size: Smaller particles are generally more difficult to wet and disperse than larger particles because of their inherently greater surface area On the other hand, smaller particles generally give MMCs with superior mechanical properties. Different SiC grit sizes were employed to produce MMCs and it was found that the finest grade(F1200-particle size 3-5μm) was the most difficult to wet and disperse in molten Al Moreover, once wetted, the F1200 grade had a greater propensity to react with molten Al. This latter effect was attributed to the larger surface area available with the finer SiC
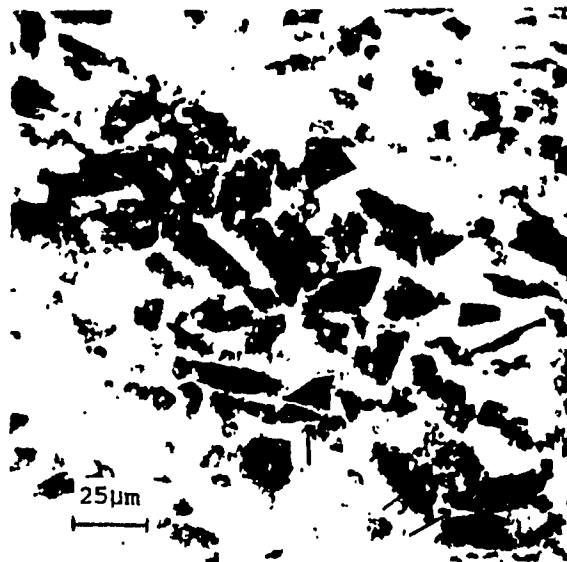
Figure 2.2   The microstructure of 6061-SiC composite The dark phase
             (arrowed) at the particle-matrix interface is the reaction product,
             Al_4C_3[28]
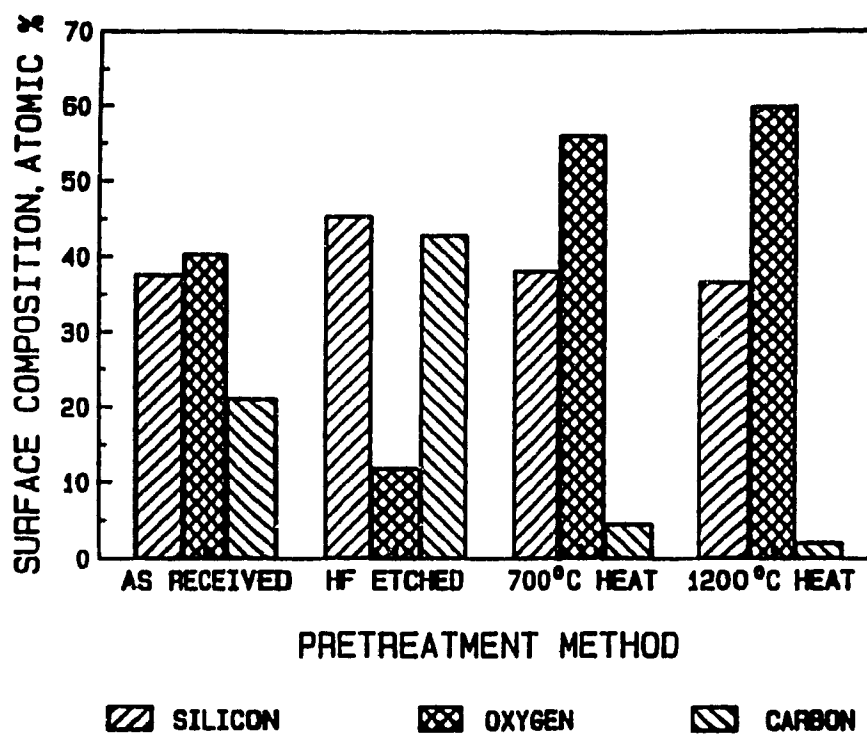
Figure 2.3   The near-surface composition of SiC particles as determined by
              XPS analysis after different surface treatment[28].

particles and consequently a higher level of surface reaction.

(c) **Variations in SiC purity level**: Both high purity grade and lower purity grade SiC were used in MMCs production. However, the difference in purity between these two grades did not have any effect on wettability or interfacial reaction in Al matrix composites.

Compared to the unreinforced alloy, SiC/Al generally offers advantages including high temperature deformation, low coefficient of thermal expansion, improved abrasion resistance and better fatigue properties[24, 25, 31]. SiC reinforcements can be in the form of continuous filaments, discontinuous whiskers or particles. The choice depends on the required properties, cost and the matrix material[24-26, 32].

Continuous filaments, ranging from 3 to 200 μm in diameter, provide the greatest improvement in strength but are also the most expensive to fabricate[24, 25, 33] Discontinuous whiskers are needle-like fibers with very small diameters and lengths ranging from 10 to 100 μm. The length to diameter ratio of these crystals is typically between 50 and 150. Whiskers are used to produce the highest strength discontinuous reinforced metal matrix composite[25, 31, 34]. Particles provide the least improvement in strength and stiffness but are the least expensive reinforcement to produce. Ranging in diameter from 3μm go to 200 μm, they produce more isotropic properties, while continuous fibers and discontinuous whiskers yield more directional properties [24,25] Using particles of around 10 μm reduces the propensity for particle fracture which occurs readily in coarse particles. The composite ductility is very sensitive to the distribution of particles, with voids opening up in particle clusters. Since SiC particles are pushed ahead

of the liquid-solid interface, the particle distribution is dependent on the solidification conditions or casting process used. Although SiC can be used with other metals, its combination with Al alloys offers improved strength to weight ratio[24].

2.1.1.2 Al_2O_3 Reinforcement

Al_2O_3 in fiber form has been used widely for making the fiber reinforce composite [35]. The two continuous Al_2O_3 fibers that are currently commercially available are Fiber FP from Du Pont [36, 37] and Sumika from Sumitomo [38]. These multifilament yarns contain at least 85% Al_2O_3. Saffil [39], a short staple fiber manufactured by ICI, also has been evaluated in many of the same applications as have the continuous fibers [40]. The physical properties of these important alumina fibers are given in Table 2.1. The development of Al_2O_3 fiber reinforced MMCs has focused on the low melting point metals, such as aluminum and magnesium and their standard casting alloys. Little has been done with steel and superalloy composites because Al_2O_3 fibers tend to undergo degrading microstructural changes at the required fabrication and creep application temperatures. In addition, forming operations such as forging or rolling would break the fibers. While composites could be made by casting, the temperature (1600°C) and the aggressive reactivity of molten iron would cause grain growth and chemical attack of the Al_2O_3. In the case of superalloys, composites could be formed by plasma spraying or diffusion bonding, but these alloys are generally used in applications requiring temperatures of 1000°C and above. At these service temperatures, most Al_2O_3 fibers will eventually lose strength through grain growth and will creep under load.

Table 2.1   Properties of current aluminum oxide fibers[1]

Fiber	Composition, %		Crystal	Filaments/	Fiber φ	Density	Tensile	ψ	Modulus	CTE
	Al_2O_3	SiO_2	form	yarn	μm	g/cm3	σ,MPa	%	GPa	
Fiber FP	99.5	....	α	200	20	3.9	1560	0.4	390	6.8
Sumika	85	15	γ	380	17	3.2	1775	0.8	210	8.8
Saffil	96-97	3-4	δ	380	3	3.3	2000	0.7	300	

Alumina(Al_2O_3), is perhaps the material most commonly used in the production of technical ceramics. The reasons for its wide acceptance are many; alumina has a high hardness, excellent wear and corrosion resistance, and low electrical conductivity It is also fairly economical to manufacture, involving low-cost alumina powders[41].

Investigations on the Al/Al_2O_3 system have indicated that various chemical reactions can occur between matrix and particles depending on the nature of the matrix. Levi et al.[42] studied reactions in $Al-Mg/ \alpha-Al_2O_3$ and $Al-Cu/\alpha-Al_2O_3$ systems and found that an interaction zone occurred between the matrix and the $\alpha-Al_2O_3$ short fibers A high concentration of Mg or Cu was detected within the reacted zone. The products of the reactions were identified as either $MgAl_2O_4$ or $CuAl_2O_4$ from reactions such as:

$$3Mg + 4Al_2O_3 = 3MgAl_2O_4 + 2Al \qquad (2.2)$$

and

$$2Cu + O_2 + 2Al_2O_3 = 2CuAl_2O_4 \qquad (2.3)$$
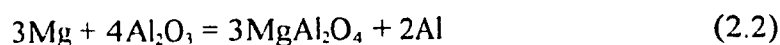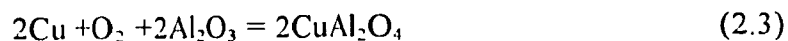
The spinodal structure of $MgAl_2O_4$ was later confirmed by electron diffraction [43]. In a system of $Al-Mg / \alpha-Al_2O_3$ particles, Karlsen et al. [44] also observed the formation of $MgAl_2O_4$ at the interface. They further noted that the dispersion of Al_2O_3 particles in Al-Mg melt was enhanced by increasing Mg content of the melt.

Hall and Barrailler[45] found that when $\alpha-Al_2O_3$ fibres were brought in contact with an Al-Li melt, a thin layer (50-200nm thick) consisting of $\alpha-LiAlO_2$ and $LiAl_5O_6$ formed at the intterface. The reaction layer grew to more than 6µm after further exposure at 500°C for 100 hours, accompanied by a degradation of mechanical properties.

The matrix / particle reaction kinetics may be related to the form of the Al_2O_3 particles used. Some Al_2O_3 particles (under-sintered) display very rough surfaces and fine grain sizes. The rough surfaces give rise to large surface area in contact with the alloy melt. Fine grains in turn mean more grain boundaries which are vulnerable to attack and serve as penetration paths for reactions. Therefore such particles react easily In contrast, Al_2O_3 particles of low surface area and coarse grain size e.g. fused Al_2O_3 tend to be more resistant to attack by the melt.

2.1.2 Fabrication

Usually continuous fiber MMCs are made by casting, which avoids the fiber damage encountered in mechanical-forming operations, such as forging and powder metallurgy. Casting also permits production of near-net shape components that require little machining One of earliest fabrication developments in this area was vacuum infiltration casting, a process in which molten metal is drawn into an evacuated mold containing a fiber perform[46]. To use the method successfully with aluminum, a small amount of lithium is added to the matrix metal to promote fiber wetting and produce a porosity-free composite. Squeeze casting has also been employed to ensure good infiltration of the metal into a fiber perform[47]. Squeeze casting does not require special alloys and is more amenable to high-production casting operations. Both methods use process optimization to produce superior composite properties. Considerable attention has been given to the role of the rate of solidification in development matrix microstructures in cast composites[48].The presence of fibers in these composites also has significant impact

on the microstructure, as do chemical reactions between the fibers and matrices[49, 50]. The fibers have been found to control the location and distribution of phases in the matrix and to direct or disrupt dendrite growth. The surface of the fibers can act as an nucleation catalyst, for solidification processing, and the fiber-matrix interface is often the site of reactions that occur during processing.

Alcan obtained the technology for manufacture of aluminum composites via a stir casting approach known at the time as the "Dural Process [51]". Since the composites are produced in the molten state, they can be processed using conventional casting and fabrication techniques and can also be cast to shape. However, problems of segregation occur as the particles increase in size and volume fraction [4, 5, 7]. The uniformity of distribution is improved by faster cooling to reduce the spacing of the dendrite arms. In the DURALCAN product lines, the Al_2O_3/Al alloys are produced in the form of extrusion billets[51]. The high-volume, raw material production decision dictated that this composite extrusion billet be fabricated using the Direct Chill casting process which is the aluminum industry standard for extrusion billet and sheet ingot. The modification of conventional DC casting processes to accommodate the composite material was a sizable development effort and its success is considered central to the commercial feasibility of DURALCAN extrusion billet. Large volume extrusion dictates the use of shear-faced dies rather than lubricated, conical dies which have often been used with metal composites. The abrasive action of the Al_2O_3 particles on the extrusion dies is a primary concern. The problem of die wear is magnified in a large volume product; even if one could tolerate the

costs of regular replacement of the tool steel dies, die production capacity could be a major challenge[51].

Powder Metallurgy (P/M) (Figure 2.4) to produce Al_2O_3/Al needs long processing time, but it is more economical for making complex parts and small objects. P/M route begins with the mixing and blending of pre-alloyed metallic powder and ceramic material, followed by pressing and sintering of the constituent powders and finally consolidation into intermediate or final product forms[5, 7, 31]. Huda et al.[27] stated that the addition of 1% lubricant to Aluminum Matrix Composite powder is good practice in order to give the compact enough strength for handling and to lubricate the die walls to facilitate pressing as well as ejecting the compacted part. However the presence of lubricant in the finished part is not desirable, hence it should be burnt off before sintering takes place. The burning off temperature for lubricant is between 430°C to 540°C depending on lubricant type and sintering atmosphere[52]. The primary requirement for a good composite structure is homogeneous distribution of the reinforcement in the matrix This is achieved by a proper choice of blending time and rotation of the mixture[53]. Pure Al powder was used as the matrix element and Al_2O_3 powder of mean particle size 45 μm in different volume fraction was used as the reinforcement element. Zinc stearate was usually used as a lubricant to reduce the friction during compaction and ejection. It is very difficult to make the composite with high volume fraction of reinforcement by P/M method[54] However repressing and re-sintering may improve the strength of the composite. The ceramic powders employed sometimes may be finer(about 5μm) than those in solidification processing. This process is unlikely to yield complete density of the powders
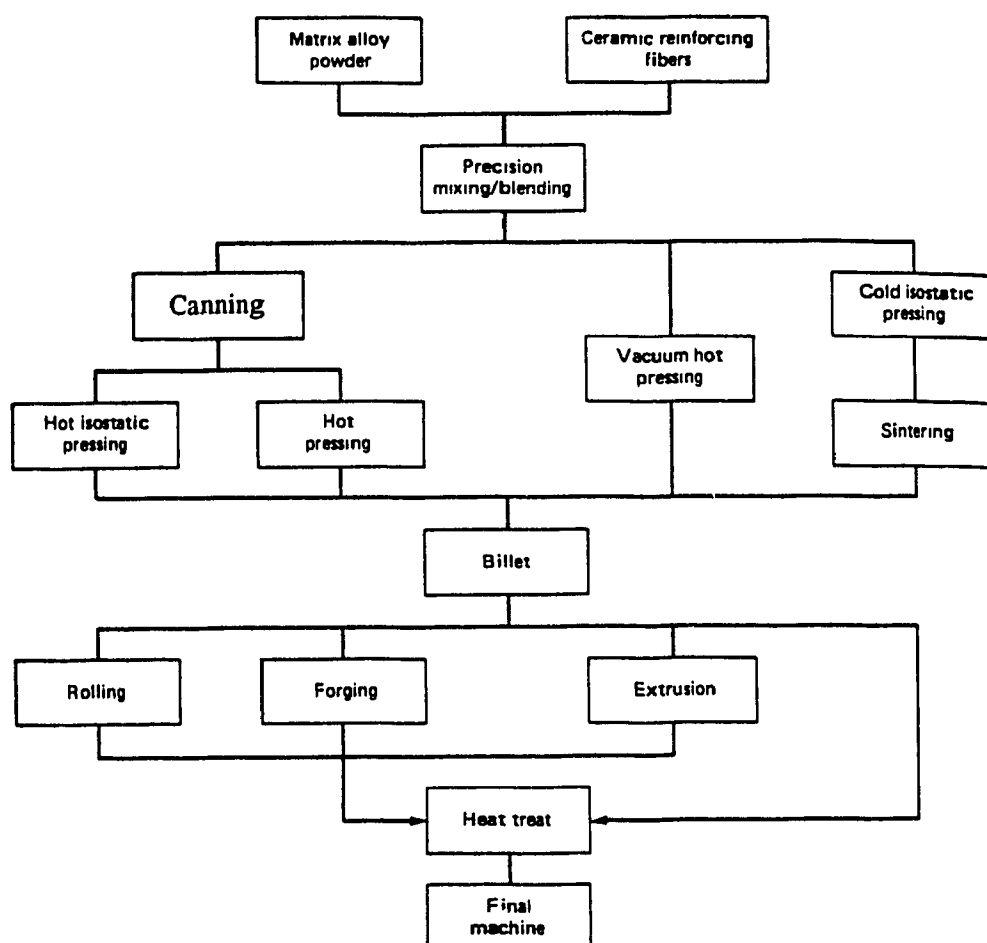
Figure 2.4   Powder metallurgy fabrication route for discontinuously reinforced composites[55]

if the initial compaction is cold which can mechanically damage the reinforcements Hot

isostatic pressing is an effective process in eliminating voids with limited damage [5, 7]

P/M manufacture generally yields improved mechanical properties compared to liquid melt

fabricated composites. When composites are produced by P/M, the reinforcement is either

never exposed to molten metal or exposed to short contact times during sintering

However, in molten metal processing, because of the relatively long exposure times, the

liquid metal may react with the reinforcing material and degrade it[55]

2.1.3 Mechanical Properties

The mechanical properties of Al_2O_3 reinforced aluminum are better than those of

the unreinforced advanced alloys in several ways, being stronger and more wear resistant

The enhanced properties of the composites allow for the use of components with lower

sectional thickness and therefore less weight. Unfortunately, these advantageous

properties are accompanied by low ductility and fracture toughness[31, 33]

Composites respond very well to heat treatment Figure 2.5 shows that aging times

to achieve peak strength are reduced for SiC/Al composites[56]. The difference in aging

behaviour of the reinforced materials and the unreinforced alloys suggest that the matrix

behaves in a particular way, as a consequence of the presence of the reinforcement[57]

The increase in yield stress and the reduced aging time is attributed to the presence of high

diffusive interfaces in the composite and to the high dislocation density as a result of the

differences in coefficients of thermal expansion of the matrix and the reinforcement[57].
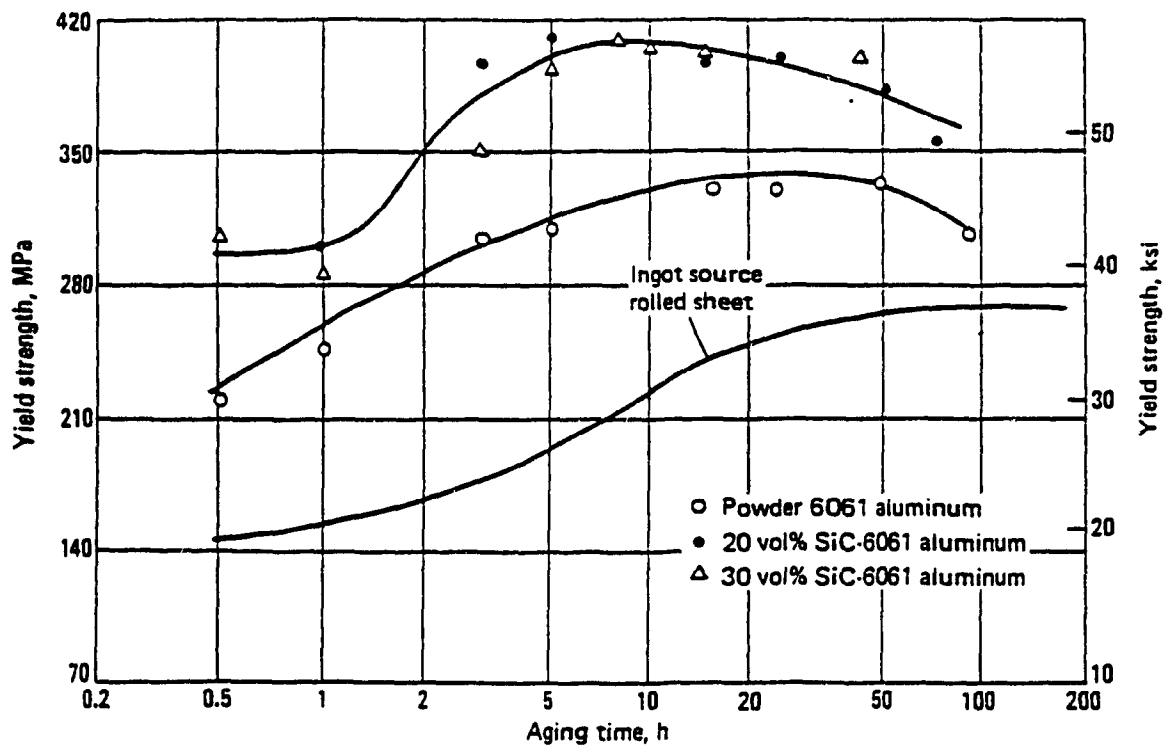
Figure 2.5   Aging response for 6061 Al and SiC/6061 Al Composites, age at 160°C[56].

2.2 Aluminum Matrix Alloy (7xxx Series)

It is known that 7xxx series aluminum alloys exhibit a low ductility in high temperature industrial processing. This property is strongly influenced both by inter and intragranular precipitates, dispersoids and grain size and by the processing sequence used to shape the components. Zinc, in amounts of 1 to 8%, is the major alloying element in 7xxx series alloys, and when coupled with a small percentage of magnesium results in heat treatable alloys of moderate to very high strength[58].

These alloys represent the high strength Al alloys in which the main strengthening precipitate is $MgZn_2$(the metastable form of this phase imparts the greatest strength). The experience to date with SiC reinforced 7xxx series alloy is that the strength of the MMCs is lower than that of the matrix alloy after identical T6 heat treatment (Table 2 2) This observation is supported by a publication[59] in which the tensile properties of 7091-20%SiC are shown to be lower than those of unreinforced 7091[28].

In peak-aged condition, the presence of the equilibrium form of the $MgZn_2$ precipitates has been observed at the matrix-particle interfaces[60]. This means some Mg is locked at the interfaces and hence is not available to strengthen the matrix Although addition of extra Mg compensates for the Mg tied up in Mg_2Si and epuilibrium $MgZn_2$ at interfaces, the necessary balance between the various alloying additions can be destroyed For instance, if the Mg Zn ratio becomes too low, the metastable precipitate may not form. Furthermore, properties such as stress corrosion susceptibility can be adversely affected. Hence, the 7xxx series alloys need greater care when used as matrices for

Table 2.2   Room temperature properties of extrusions based on 7xxx series alloys

(T6 Condition)[28]

	0.2% Proof Stress (MPa)	U.T.S (MPa)	Elongation (%)
7075	565	650	9.4
7075+10%SiC	420	516	3.0
7091	520	590	10.2
7091+20%SiC	400	470	1.9

MMCs.

7xxx series alloys aged to maximum strength exhibit reduced resistance to stress corrosion cracking and are often utilized in a slightly overaged temper to provide better combinations of strength, corrosion resistance, and fracture toughness.

2.2.1 Age-Hardenable Al Alloys

The mechanism of strengthening by age hardening involves the formation of coherent clusters of solute atoms (that is, the solute atoms have collected into a cluster but still have the same crystal structure as the solvent phase). This causes a high local strain field because of mismatch in size between the solvent and solute atoms. The cluster stabilizes dislocation, because dislocations tend to reduce the strain, similar to the reduction in strain energy of a single solute atom by a dislocation. When dislocation are anchored or trapped by coherent solute clusters, the alloy is greatly strengthened and hardened[58].

However, if the precipitates are semicoherent (sharing a dislocation-containing interface with the matrix), or incoherent (sharing a disordered interface, akin to a large-angle grain boundary, with the matrix), or they are incapable of reducing strain energy because they are too strong. Dislocations bow into a roughly semicircular shape between the particles under the action of an applied shear stress. This leaves loops of dislocations around the particles which cause a high rate of strain hardening. Consequently, the presence of the coherent particles surrounded by the strain fields in the matrix and the precipitate particles provides higher strength by obstructing and retarding the movement

of dislocations. The characteristic that determines whether a precipitate phase is coherent or noncoherent is the closeness of match or degree of disregistry between the atomic spacings on the lattice of the matrix and on that of the precipitate[58].

The hot working range of age-hardenable Al alloys lies between 200 and 500°C that is approximately between the solvus and the artificial aging temperature. The high strength is produced by the finely dispersed precipitates that form during aging heat treatments which may include either natural aging or artificial aging. This final step must be accomplished not only below the equilibrium solvus temperature, but below a metastable miscibility gap called the Guinier Preston(GP) zone solvus line. The supersaturation of vacancies allows diffusion, and thus zone formation, to occur much faster than expected from equilibrium diffusion coefficients. In the precipitation process, the saturated solid solution first develops solute clusters, which then become involved in the formation of transitional precipitates. The final structure consists of equilibrium precipitates, which do not contribute to age hardening[58].

Natural aging refers to the spontaneous formation of a G-P zone structure during exposure at room temperature. Solute atoms either cluster or segregate to selected atomic lattice planes, depending on the alloy system, to form the G-P zones, which are more resistant to movement of dislocations through the lattice, and hence are stronger Curves showing the changes in tensile yield strength with time at room temperature(natural aging curves) for three commercial heat-treatable alloys of different alloy systems are shown in Figure 2.6 The magnitudes of increase in this property are considerably different for the three alloys, and the differences in rate of change with time are of practical importance.

Because 7075 and similar alloys never become completely stable under these conditions, they are rarely used in the naturally aged temper. On the other hand, 2024 is widely used in this condition.

Artificial aging includes exposure at temperatures above room temperature so as to produce the transitional(metastable) forms of the equilibrium precipitate of a particular alloy system. These transitional precipitates remain coherent with the solid-solution matrix and thus contribute to precipitation strengthening. With further heating at temperatures that cause strengthening or at higher temperatures, the precipitate particles grow, but even more importantly convert to the equilibrium phase, which generally are not coherent These changes soften the material, and carried further, produce the softest or annealed condition. Even at this stage, the precipitate particles are still too small to be clearly resolved by optical microscopy, although etching effects are readily observed-particularly in alloys containing copper[58].

Precipitation heat treatment or artificial aging curves for the Al-Mg-Si alloy 6061 are shown in Figure 2.7 This is a typical family of curves showing the changes in tensile yield strength that accrue with increasing time at each of a series of temperatures. In all cases, the material had been given a solution heat treatment followed by a quench just prior to the start of the precipitation heat treatment[58].

The hot working is usually carried out in material that has been overaged or equilibrium precipitated by slow cooling. In such condition, the alloys are usually stronger than pure Al but have an activation energy, Q_{hw}, which is almost the same However, when these alloys are worked in the solution treated condition, they exhibit much higher

Q_{hw}, much greater peak stress σ_p and work softening, $\Delta\sigma$, lower ductility and less recovered substructure than the material with medium precipitates that have little interaction with dislocations[61].

The 7xxx series of age-hardenable alloys that are based on the Al-Zn-Mg-Cu system develop the highest room-temperature tensile properties of any aluminum alloys produced from conventionally cast ingots[58]. However, the strengths of these alloys decline rapidly if they are exposed to elevated temperatures (Figure 2.8), due mainly to coarsening of the precipitates on which the alloys depend for their strength.
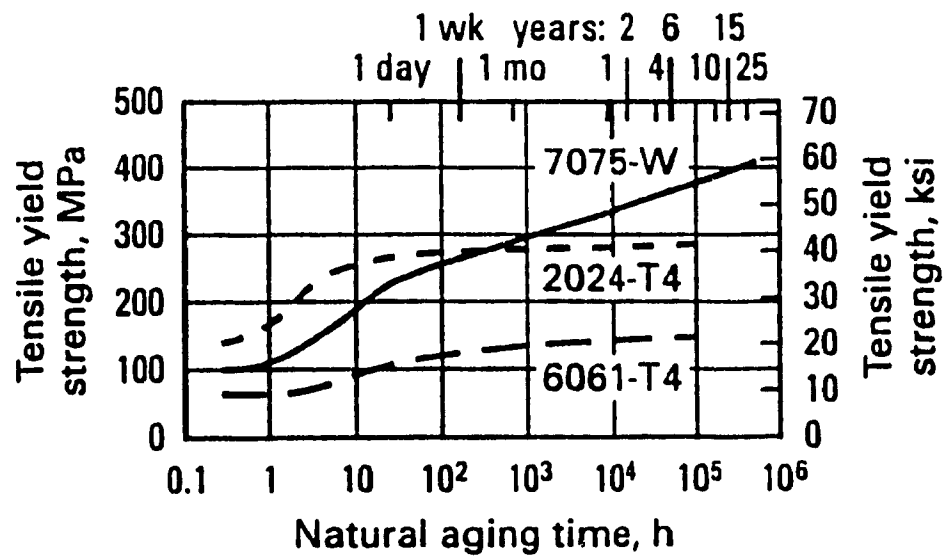
Figure 2 6   Natural aging curves for three solution heat-treated wrought
aluminum alloys[58]
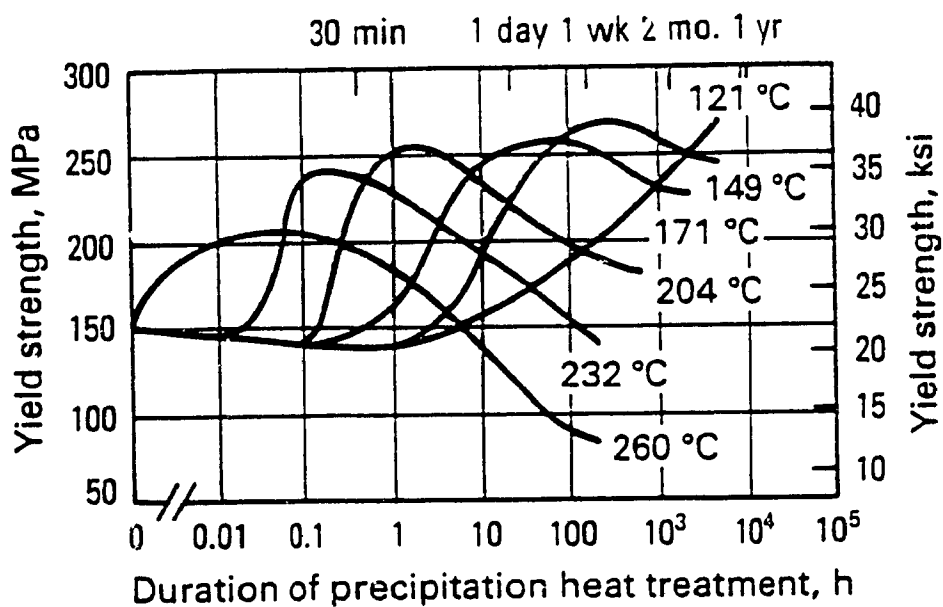
Figure 2 7   Precipitation heat treatment or artificial aging curves for solution
             heat-treated aluminum alloy 6061[58]
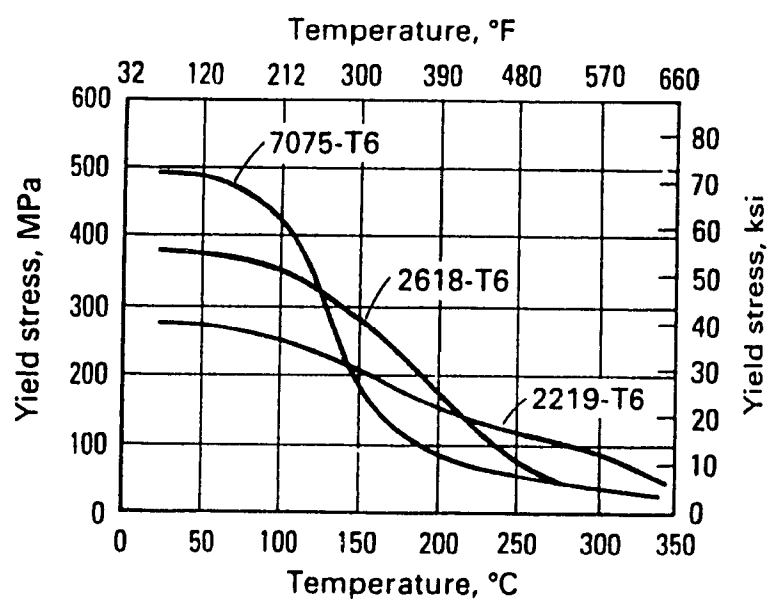
Figure 2.8   Values of 0.2% yield stress of aluminum alloys after exposure for 1000 h at temperatures between 0 and 350°C [58]

3. HOT WORKING CHARACTERISTICS

Hot working is considered to be deformation at a temperature above 0.5 T_m (melting temperature, K) and strain rate between 10^{-3} to 10^3 s^{-1}. The strains may vary from 0.1 to as high as 50. At these temperatures, most metals have a low flow stress and a high ductility. Both dynamic and static softening mechanisms take place during the hot working process which includes the preheating, deformation and subsequent cooling. Hot working is employed because metals can be subjected to large and rapid changes in shape without cracking. The perennial need for improved processes and products generates continued and growing interest in high temperature deformation[62, 63].

3.1 Restoration Mechanisms on Hot Working

Hot deformation of any metal will cause an increase in dislocation density within its grains, which serves to strain harden the material and will ultimately lead to fracture if some form of restoration mechanism is not active to alleviate stress concentrations. Since hot working is generally performed in several steps, the restoration processes can be divided into two main groups: those occurring during deformation are called dynamic and those taking place in the absence of stress or strain on the material are termed static. In any deformation process, one or all of the following restoration mechanisms may be active·

(i)   Dynamic Recovery (DRV)

(ii)   Dynamic Recrystallization (DRX)

(iii)   Static Recovery (SRV)

(iv)   Static Recrystallization (SRX)

The major factor that determines whether recovery or recrystallization will take place during hot working is the stacking fault energy (SFE). Their initiation and control is dependent on both material properties and on the selection of such parameters as temperature, strain, strain rate and time[62, 63]. For high SFE metals, only DRV is observed. However, for metals of moderate or low SFE, DRX takes place above a critical strain[64].

3.1.1 Dynamic Recovery (DRV)

Dynamic recovery (DRV) is the basic mechanism that leads to the annihilation of pairs of dislocations during deformation. As shown in Figure 3.1 a simple flow curve, increasing strain hardening to a steady state plateau, is characteristic of pure DRV The flow curve exhibits three distinct stages. During the first, the elastic strain is increasing from zero to the yield stress. Strain hardening takes place during the second stage, however, the slope of the curve continually decreases as the rate of work hardening diminishes. The amount of work hardening and the strain to the end of this stage decreases as the temperature is raised and the strain rate lowered. In the third stage, the work hardening rate has reached zero and the flow stress has levelled off at an equilibrium steady state value. Therefore, in hot working, the temperature, the strain rate and the flow stress are constant in the steady state regime. In practice, the flow curve may decrease
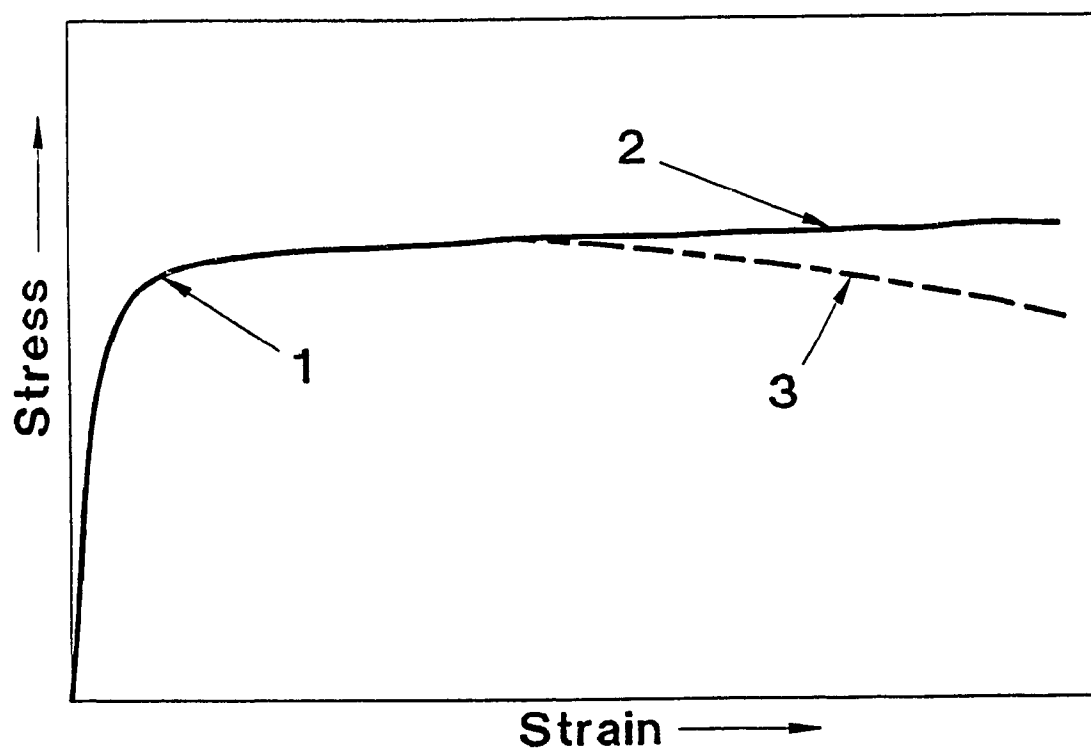
Figure 3.1   Typical dynamic recovery flow curve: after an initial strain
hardening phase (1), there is a region of steady state deformation
without strain hardening (2), In practice, the flow curve may
decrease as the result of deformation heating or precipitate
coalescence (3)[65].

after the plateau has been reached as the result of other factors such as deformation heating or precipitate coarsening[62,63, 66].

During the initial loading stage of the flow curve, some dislocation multiplication takes place, increasing slightly the dislocation density. In the strain hardening stage, the dislocations increase greatly and become entangled into a substructure within the grains As deformation continues in metals with high SFE, the sub-boundaries increase in number and dislocation density and rearrangements by DRV also rise until a dynamic equilibrium is reached between dislocation generation and annihilation. At this point where the subgrains reach the equilibrium size, a steady state is established in which the flow stress remains constant. While the grains are deforming in correspondence with the external shape, the subgrains remain equiaxed even after large strains, indicating that the individual sub-boundaries are being broken up and reformed This dynamic regeneration termed repolygonization explains the absence of any distorted subgrains even after very large strains. The subgrains become larger in size as the deformation temperature is increased or as the strain rate is decreased. Such larger subgrains and their boundaries, both contain less dislocations[62, 63, 66, 67].

The description of DRV up to this point refers to metals in which it occurs to a high degree. In the case of two-phase alloys, where the particles are small and insoluble and are not sheared by the dislocations, they serve as obstacles which stabilize the substructure. Examples of this are fine equilibrium Mg_2Si precipitates or $FeAl_i$ eutectic rods(0.2 μm). In some cases the subgrain diameter may be reduced to the size of the inter-particle spacing which led to high flow stresses. However, when the spacing is very small,

they may inhibit the formation of subgrains; such is the case in underaged aluminum alloys If the particles are partially soluble, they can coalesce into fewer and larger particles during deformation, leading to a decreasing flow stress over a prolonged strain. At higher temperatures and lower strain rates, the particles are larger when steady state flow is achieved. Fine and uniformly distributed particles which would limit the degree of recovery, tend to decrease the ductility. Large non-deformable particles such as constituent $MnAl_6$ or α-AlFeSi (> 0.6 μm) or SiC particles in MMCs cause additional deformation in the surrounding matrix and the development of very fine subgrains The dense dislocation substructure can give rise to particle stimulated nucleation(PSN) of recrystallization. Large particles can also lead to the nucleation of voids or cracks which then link up to cause failure. If the amount of particles is high, then the crack density may be so great that their growth counters the ductility enhancement of the recovery or recrystallization mechanisms[66, 67].

3.1.2 Dynamic Recrystallization(DRX)

The typical flow curve of a material undergoing DRX is shown in Figure 3 2 Several distinguishing characteristics of the Figure 3.2 are:

(i)   The initiation of recrystallization after a critical strain denoted by a decrease in work hardening rate to a distinct peak in the flow curve

(ii)   A flow softening due to the growth of DRX grains which are also being deformed.

(iii)   The flow stress levelling off at a steady state value due to strain hardening,
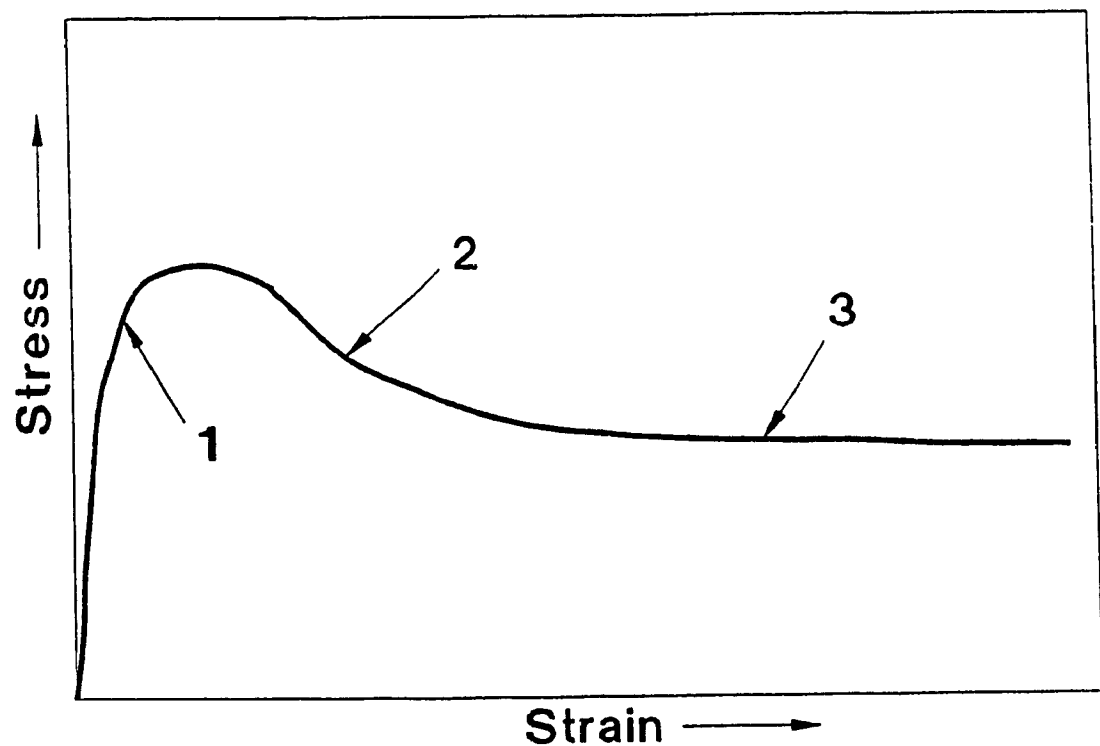
Figure 3.2   Typical dynamic recrystallization flow curve: the accumulation of
              dislocations is sufficiently great that recrystallization is nucleated
              during deformation (1). Since the recrystallized grains have a lower
              density of dislocations (2) than the unrecrystallized material (1),
              there is work softening. These recrystallized grains are continually
              reworked and repeatedly recrystallized giving the steady state flow
              stress (3)[65].

DRV in the new grains and repeated uniformly distributed DRX.

At higher strain rates, DRX is continuous after giving rise to a single peak stress value and produces grain refinement. However, at lower strain rates, the mechanism is periodic with each stress-decreasing recrystallization wave followed by a degree of work hardening. The result is a cyclic pattern of decreasing amplitude and grain coarsening [89-93].

DRX is generally observed in metals with low SFE whereas in metals with high SFE, it seldom occurs because DRV produces a low dislocation density. When the dislocation density builds up to a critical level, it is the critical strain at which DRX occurs. At lower strain rates nucleation possibly occurs by the bulging of existing grain boundaries. Migrating grain boundaries leave behind dislocation-free regions in which the dislocation density once again increases as strain proceeds until recrystallization is again nucleated. At high strain rates, a fine and dense tangled cellular structure is developed throughout the grains but more strongly at the grain boundaries and deformation bands. Nuclei develop initially along grain boundaries where there are high misorientations between the subgrains. The dislocation densities at the center of the new grains increase sufficiently that nucleation occurs again before any wave of recrystallization is complete. As a result, there is a distribution of dislocation substructures which maintains the average flow stress at a steady state between the yield stress of statically recrystallized material and the peak stress [89-93].

3.1.3 Static Recovery(SRV) and Static Recrystallization(SRX)

At the end of a high temperature deformation, there is a dislocation substructure with an associated stored energy which is capable of driving static restoration mechanisms such as SRV and SRX[94, 95].

SRV is the annihilation and rearrangement of dislocations in the sub-boundaries followed by growth of the subgrains. This process is the sole mechanism of softening if the critical stored energy is not surpassed and always occurs during the incubation period before the appearance of recrystallization nuclei. As the stored energy increases, the incubation period for SRX decreases so that there is less opportunity for SRV An increase in temperature or strain energy (higher ε or $\dot{\varepsilon}$) increases the rate of SRV while the addition of alloying elements decreases it [94,95].

SRX is the elimination of dislocations as a result of the motion of high angle boundaries. SRX is preceded by an incubation period for nucleation, i.e. formation of regions with low dislocation density surrounded by mobile high angle boundaries The new grains grow until all the deformed grains are replaced. A critical strain is required for SRX to take place; it rises as the temperature rises and the strain rate falls. At higher strains or strain rates, the driving forces are higher making the rate of recrystallization faster. Part of this results from the reduction of the subgrain size and increase in sub-boundary density so that there is a higher density of nucleation sites [63, 78, 95].

The effects of second phases are varied depending on their size and spacing If they are small and numerous, they tend to stabilize the substructure, thus both limiting SRV and preventing nucleation of recrystallization. Larger particles distributed along the grain

boundaries, may prevent their migration and consequently recrystallization without altering recovery. However, large and rigid particles (>0.6 μm) which cause additional flow in the surrounding matrix, create nucleation sites for SRX [17].

3.2 Interdependence of Stress Rate and Temperature

A number of mathematical expressions have been proposed to describe the relationship between flow stress (σ), strain rate (ε̇) and temperature (T in Kelvin). In creep, the increase of ε̇ in the steady state region as T rises and σ increases can be expressed by a power law and an Arrhenius relationship:

$$\dot{\varepsilon} = A_1 \, \sigma^{n'} \exp(-Q_c/RT) \qquad (3.1)$$

where
A_1 : Empirical Constant

R : Universal Gas Constant (8.314 J/mol-K)

Q_c : Activation Energy for Creep

For aluminum, the relationship holds over eight orders of magnitude from 10^{-8} to 10^{-2} s^{-1}. The value of Q_c is approximately equal to that for self diffusion indicating that the rate controlling mechanism is dependent on vacancy migration [17, 62, 63, 65-67].

The interrelationship between the three parameters σ, ε̇ and T can also be written in the hot working form and with different stress functions:

$$A_1 \, \sigma^{n'} = \dot{\varepsilon} \exp(Q_{HW}/RT) = Z \qquad (3.2)$$

$$A_2 \exp(\beta\sigma) = \dot{\epsilon} \exp(Q_{IIW}/RT) = Z \qquad (3.3)$$

$$A_3[\sinh(\alpha\sigma)]^n = \dot{\epsilon} \exp(Q_{IIW}/RT) = Z \qquad (3.4)$$

where A_i, α, β, n, n'   : Empirical Constants

               Z   : Zener-Hollomon Parameter

               Q_{IIW} : Activation Energy for Hot Working

These equations hold for DRV or DRX but Q_{IIW} would be different for the two mechanisms. The power law (Equation 3.2) works satisfactorily for low stresses and the value of n is usually in the range of 4 to 5. The exponential law (Equation 3.3) is useful for high stresses and β (= αn') has values in the range of 1 to 1.5×10^{-1} MPa^{-1}. The hyperbolic sine law (Equation 3.4) covers the entire stress range (10^8 to 10^2 s^{-1})(Figure 3 3) The Z parameter is a temperature compensated strain rate which increases as T decreases. In hot working tests, Z is constant since T and $\dot{\epsilon}$ are the controlled variables [17, 62, 63, 65-68]

3.3 High Temperature Deformation of Particulate AMC

The mechanical behavior of particulate AMC at high temperatures is very important since they may be produced as billets which are subsequently mechanically shaped.

Deformation processing of discontinuously reinforced composites is usually carried out at higher temperatures where the ductility is greater and the flow stress lower although it remains significantly higher than that of the matrix alloy[7-9, 11-13, 15]. The reinforcing
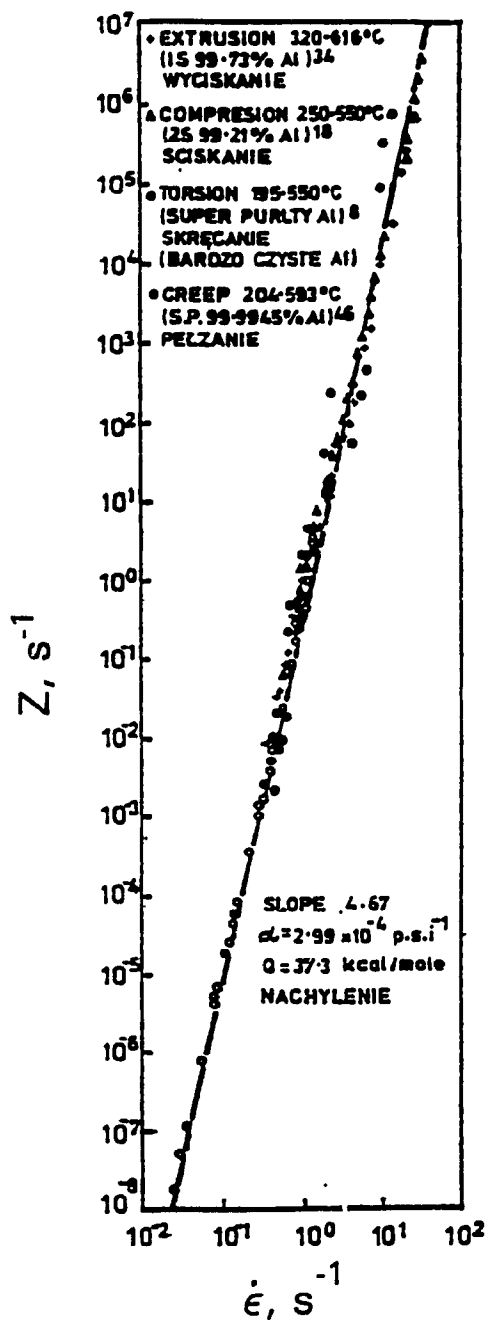
Figure 3.3   The application of Equation 3.4 to aluminum is confirmed over the strain rate range 10^{-2} to 10^{2} s^{-1} between 195 and 616°C[68].

particles reduce the workability because of the initial high dislocation density, introduced by their difference in thermal expansivity (ΔCTE) from the matrix and by the constraints to plastic flow arising from their relative rigidity[69]. Usually the AMC matrices include medium strength 6061 (Mg_2Si precipitates), casting alloy A356 strengthened by Si eutectic particles and high strength 7075 (($MgCu)Zn_2$ precipitates)[18] The reinforcements involve both SiC and Al_2O_3 of about 18 μm diameter in concentrations of 10, 15 or 20 v%. Above 200-300°C, the work hardening rate of the matrix alloys are reduced primarily by DRV[7, 8, 14, 15,].The particles in composites are sufficiently large that they do not interact with dislocations but being much harder than the matrix, they do force it to undergo additional shear thus raising the strain hardening[7, 8, 15,] At temperatures near melting (aluminum: Tm = 660°C), the flow stress of the composite may fall below that of the matrix alloy and the strain rate sensitivity may increase. These effects have been attributed to grain boundary sliding in fine grained composites[7, 9]. Powder based composites are usually hot worked following consolidation to improve the mechanical behavior by eliminating unmixed regions of reinforcement and matrix thus augmenting the reinforcement-matrix bond. The distribution of the second phase in the matrix becomes more uniform as the amount of deformation is higher. Elevated temperature improves matrix flow and reduces particle degradation[4, 5, 10, 14, 70]. Such behavior in hot working indicates that it would be much more suitable than cold working for fabrication of composites since the matrix has more ability to flow around the particles without damaging them [7, 8, 11, 14, 15].

There are distinct failure mode changes with temperature in particulate AMC. At 200-300°C, uniform elongation decreases but there is a considerable amount of necking and the total ductility increases. At 400°C, there is a peak in the ductility as observed in Al_2O_3/7075 Al composite. The fracture surfaces of specimens are generally similar to those specimens deformed at lower temperatures, however, there is some evidence of intergranular failure at 500°C. These observations discussed above suggest that there are three distinct temperature regimes in aluminum composites[9,14]:

(i)   T < 200-300°C   High work hardening, high flow stress, low ductility

(ii) 500°C > T > 300°C   Low work hardening rate, improved ductility

(iii) T > 500°C   Lower ductility, fracture related to grain boundary
                                   sliding and cracking.

3.4 Hot Torsion Testing

The strain and strain rate obtained during tensile testing are inadequate for industrial hot forming procedures. This mode of deformation suffers from necking instability which limits the uniform strain to a low value and the number of stages to two. The microstructure in the necked region is difficult to interpret because of the strain gradients. In compression testing there is no inherent instability. However, friction between specimen and anvil usually results in severe to slight barreling. The tension test is the least useful of the three modes[71-73].

In recent years, hot torsion testing of solid cylindrical specimens has become more reliable in determining optimum hot working parameters such as strain, strain rate and temperature[18, 19, 74, 75]. Although high strains can be achieved at a constant strain rate, there is a linear variation of strain and strain rate from zero at its center to maximum at the surface. If necessary, the effects of this variation can be reduced by use of a specimen with a tubular cross section. The major advantage of torsion over tension and compression testing is that there is no change in geometry of the specimen during deformation. In light of this fact, true strain and strain rate are equal to the engineering strain and strain rate in torsion.. In the present work, the torsion test was used to determine the hot working properties of two Al_2O_3 particle reinforced 7075 aluminum matrix composites and their matrix alloy.

Computer controlled torsion testing has come to be recognized as a powerful means of assessing material behavior at elevated temperatures, particularly under the conditions of high strain and relatively high strain rate Therefore, industrial deformation processes, such at hot rolling and forging can be readily simulated Usually torsion testing data are recorded in the form of torque (Γ) versus angle of twist (θ) diagrams

The torque and twist data from the experiments were used to calculate the equivalent stresses and equivalent strains. The equivalent stress at the surface of the specimen is evaluated from the torque Γ via the relation proposed by Fields and Backofen[76]

$$\sigma_{eq} = [\ \sqrt{3}\Gamma\ (3 + m + n")\ ]\ /\ 2\pi r^3 \tag{3 5}$$

and the equivalent strain at the surface is proportional to the measured angle of twist θ, as given by:

$$\varepsilon_{eq} = r\theta/\sqrt{3}L \qquad (3.6)$$

Here, r and L are the specimen gauge radius and length, respectively, m is the strain rate sensitivity and n is the work hardening coefficient derived from the torque. These coefficients are defined as follows:

$$m = \partial\ln\Gamma/\partial\ln\theta \qquad (3.7)$$

$$n = \partial\ln\Gamma/\partial\ln\dot{\theta} \qquad (3.8)$$

Although both m and n vary with strain, for the sake of simplicity, constant values of m=0.17, and n=0.13 were employed. The variations in m and n are much smaller than the mean value of the multiplier (3+ m +n)=3.3, and the approximations, therefore, do not introduce a large error.

4. EXPERIMENTAL PROCEDURE

4.1 Torsion Testing System and Equipment

4.1.1 Hot torsion machine

Testing was conducted on a computer-directed, servo-controlled, closed loop torsion machine designed as a joint project by Sandor Fulop[77] and the Department of Mining and Metallurgy of McGill University (Figure 4.1). In this MTS electro-hydraulic system, torque is applied to a specimen through a rotary hydraulic actuator mounted on a converted lathe bed as schematically shown in Figure 4.2. The lathe bed was used as the frame of the torsion machine on which the motor-furnace-torque cell system was mounted longitudinally[96]. This motor can develop a maximum torque of 100 N.m and a maximum speed of 628 rpm. The speed and direction of rotation of the motor are controlled by a servo valve that proportions the hydraulic fluid flow to the motor in relation to the magnitude of an electrical signal. On the torsional frame, the test piece is held by two coaxial superalloy bars with attached heat resistant grips. One end of the test piece is twisted a measured amount by the hydraulic motor controlled by a servo-valve while the other end is held fixed by a torque cell.

The torque cell of 113 Nm (1000 in-lb) capacity is used to measure the load transmitted by the test piece. It is calibrated for four ranges 100, 50, 25, and 10 Nm Angular displacement is monitored by a dual gang potentiometer. They develop proportional voltages which are fed back to their respective channels in the control unit

The specimen is heated by a quadruple elliptical radiant furnace(model E4-10PA) connected to programmable controller with varied power input. The furnace is water-cooled and capable of temperatures up to 1200°C with rapid heating rates. A transparent quartz tube runs through the furnace enclosing the specimens, grips and bars. Argon is circulating through the tube during heating and testing to prevent oxidation. The temperature is measured by an alumel-chromel (K-type) thermocouple, insulated with double bore ceramic tubing, extending along the stationary test piece shoulder and attached to the specimen with alumel-chromel wire to maintain thermal contact. The location of the thermocouple tip on the gauge section at the fixed end of the specimen was determined to be satisfactory since the thermocouple could be rigidly fixed to the specimen yet underwent only a small fraction of its total revolutions without suffering damage[77]. The temperature of the test piece is displayed by a digital read-out temperature indicator[78]. The procedure of programming of the furnace temperature is provided in the Appendix. Figure 4.3 shows the picture of furnace.

4.1.2 Computerized Testing System

The torsion machine was linked to an IBM-PC compatible 486/33 Mhz. In this computer, OS/2 is employed for the operating system, together with Windows. TestStar is used to control the test procedure. Lotus 1-2-3/G was put on the hard disk for data processing. In a programmable system, the variations of all controllable parameters are entered via the program for the entire sequence which is then initiated. The responsibilities of the computer may be viewed in terms of the following four categories:
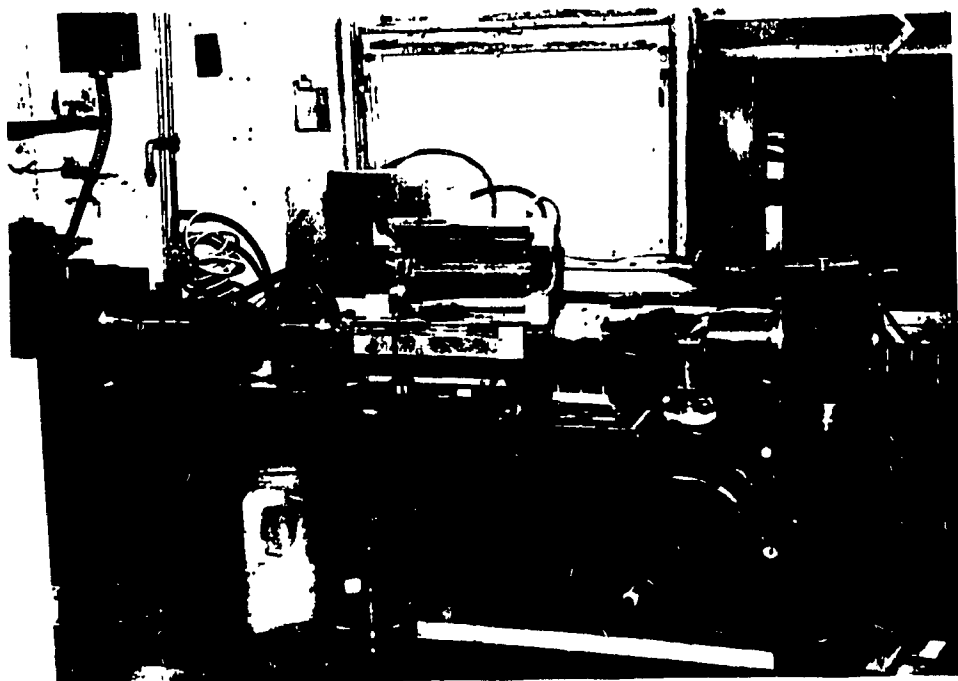
Figure 4.1   Photograph of the servo-controlled hydraulic torsion machine.
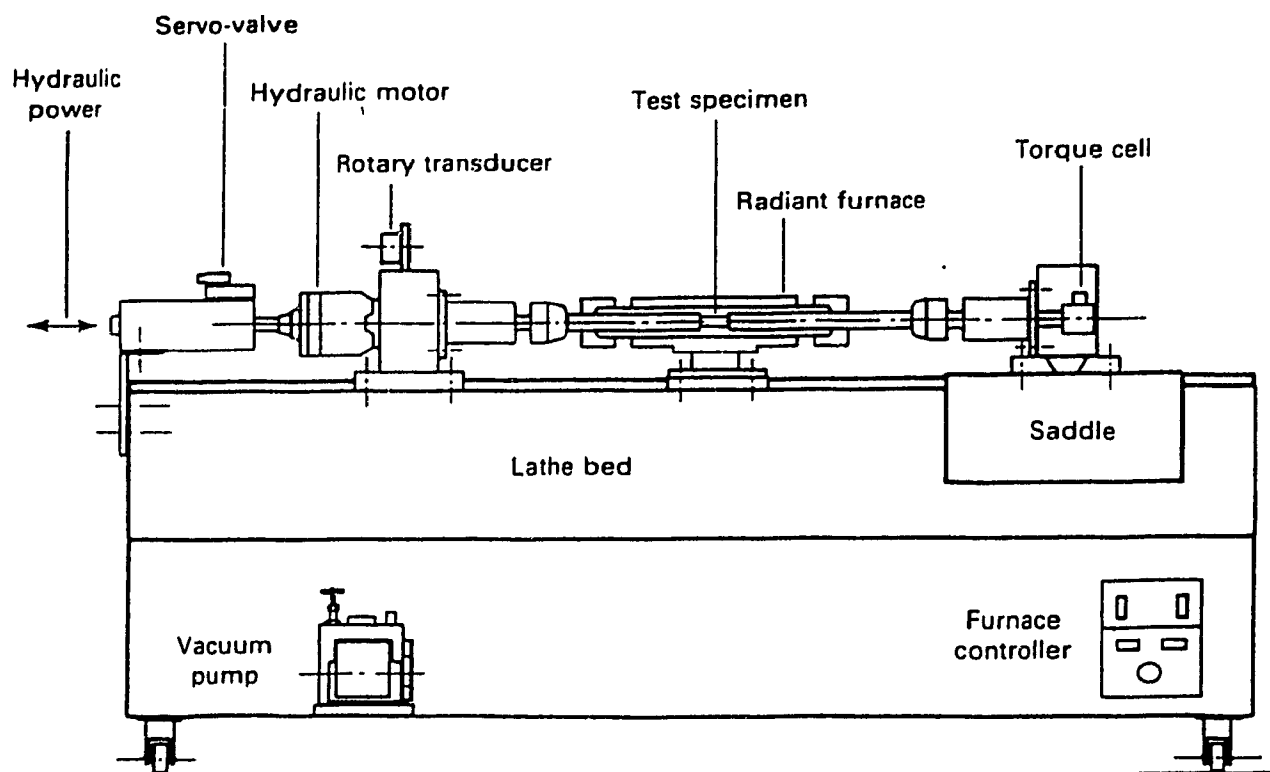
Figure 4.2   Schematic diagram of the torsion machine with the major components indicated[79].
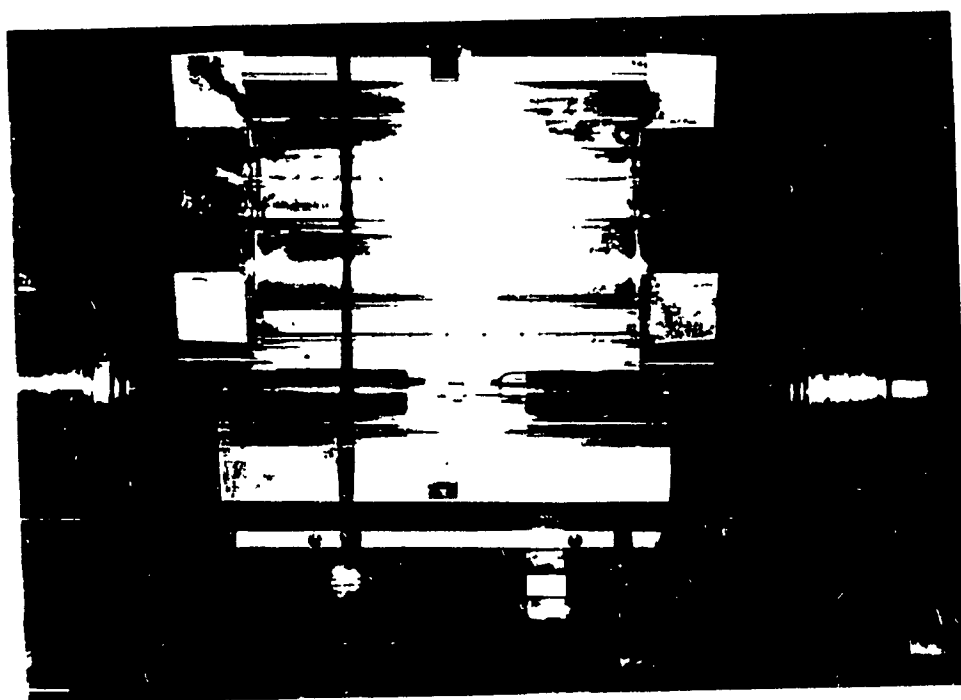
Figure 4.3   Picture of water-cooled dual elliptical radiant furnace

(i)   Accept and interpret all test parameter information from the user.

(ii) Use the input information to activate the required hardware devices which will in turn send the appropriate command signals to the closed loop system and drive the test.

(iii) Monitor and record all output feedback information from the transducers within the closed loop system as the run is being executed.

(iv) Interpret the transducer output information and arrange it so it may be presented in a legible manner to the user.

4.2 Test Materials

Three different materials were used in the present studies of which one was commercial 7075 alloy while the other two were composites of 7075 reinforced with Al_2O_3 particles of average size 12 µm to concentrations of 10% and 15% by weight. The materials were supplied in the as-cast condition by the Dural Aluminum Composite Corporation through Alcan Laboratories in Kingston, Ontario. The chemical compositions of the materials are shown in Table 4.1. Torsion specimens with axes parallel to the rolling or casting direction were machined to close tolerances, especially in gauge section, in order that twisting would be uniform. The test pieces have a gage length of 22.2 mm (0.875 in) and a diameter of 6.4 mm (0.25 in). The test specimen design is illustrated in Figure 4.4 Gage section geometry determines the deformation level and deformation rate for a given amount of twist and a given twist rate. The short lengths are used to obtain

Table 4.1   Chemical Compositions of Al₂O₃/7075 and 7075 Matrix Alloy (wt%)

Elements	Zn	Cu	Mg	Cr	Mn	Si	Fe	Al
10%Al₂O₃	5.98	1.60	2.86	0.23	0.005	0.034	0.10	Bal
15%Al₂O₃	5.82	1.51	2.75	0.23	0.006	0 038	0 10	Bal
Matrix Alloy	5.83	1.46	2.86	0.23	0.088	0.088	0 27	Bal

higher strain rates. Transition shoulders of intermediate diameter are provided between the gage length and the grip section to reduce the heat flow and the temperature gradient in the gage length.

4.3 Test Procedures

Before starting any test, the reflecting surfaces of the furnace were cleaned with gauze so that the test temperature could be reached as quickly as possible. All specimens were inserted into the grips of the bars with a high temperature anti-seize agent and were tested in a controlled atmosphere of argon to prevent contamination during elevated temperature torsion studies. One end of the test specimen is threaded to be screwed into the grip which is attached to a torque transducer fixed to the lathe bed, while the other end has a rectangular section which fits into a slot attached to the actuator[80] This arrangement allows for easy mounting and removal without accidentally straining the specimen.

Each specimen was heated to the desired temperature T within five minutes and held constant at that homogenizing temperature for ten minutes prior to deformation.. In the case of the Duralcan materials, tests were performed at three different strain rates ($\dot{\varepsilon}$) of 0.1, 1.0 and 4.0 s^{-1} and at five temperatures between 250 and 540°C. The specimens were twisted without any interruption to fracture. All specimens were quenched in water in less than ten seconds after deformation was completed. The data were stored by the computer and displayed as torque (Γ) versus angle (θ).
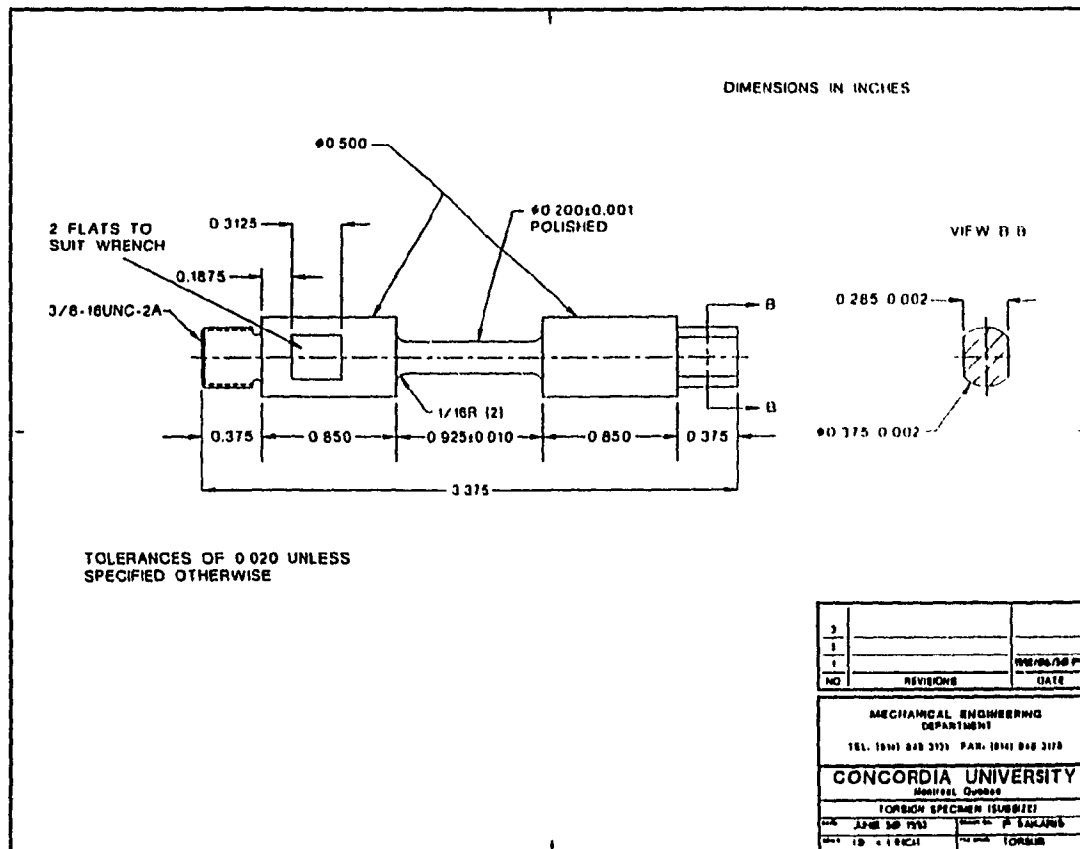
Figure 4.4   Torsion specimen design[78]

5. EXPERIMENTAL RESULTS

5.1 Data Analysis

5.1.1 Stress(σ)-Strain(ε) Curves

The torque and twist data directly from torsion testing were converted through the use of Equations 3.5 and 3.6 to equivalent stress(σ) and strain(ε), in order to compare them to the findings of other researches. In the equation used to calculate the equivalent stress, as defined in Equation 3.5, the value of n was taken as zero. This assumption is strictly valid only at the peak and during steady state. The value of the strain rate sensitivity m was taken as the slope of log Γ versus log $\dot{\varepsilon}$ (Figure 5.1). Since the m value varies with temperature as mentioned before, usually the average m value is used for simplicity in conversion of equivalent flow stress. In general, m decreases as T decreases.

The equivalent σ-ε curves for the three materials are presented in Figure 5.2. The strengths of 10% and 15% Al$_2$O$_3$ particle reinforced 7075 Al composites in comparsion to that of the unreinforced 7075 Al alloy are remarkably high at 250°C and 300°C but gradually become more similar above 400°C and even less at 500°C. The flow stresses at the peaks of the two composites and the matrix alloy decreases with increasing deformation temperature. There is a progressive rise in peak flow stress when the strain rate is increased for all temperatures. At all temperatures, all materials strain harden to a maximum, then the flow stress gradually declines until failure occurs. In general, more flow softening toward a steady state regime before fracture is observed to be higher than
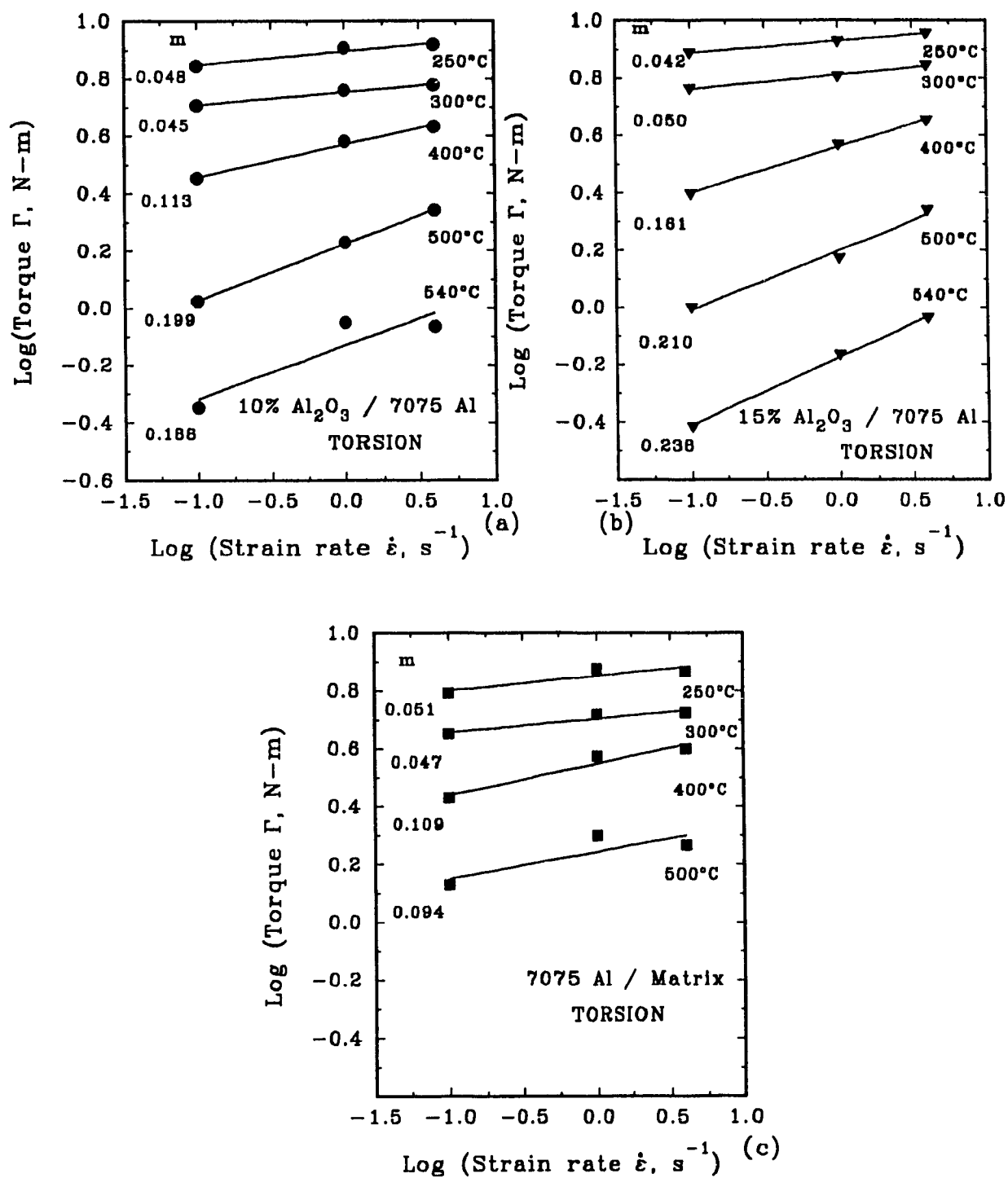
Figure 5.1   Plot of log Γ versus log ἐ was used to calculate m for: (a) 10% Al₂O₃/7075 Al, (b) 15% Al₂O₃/7075 Al, (c) 7075 matrix alloy.
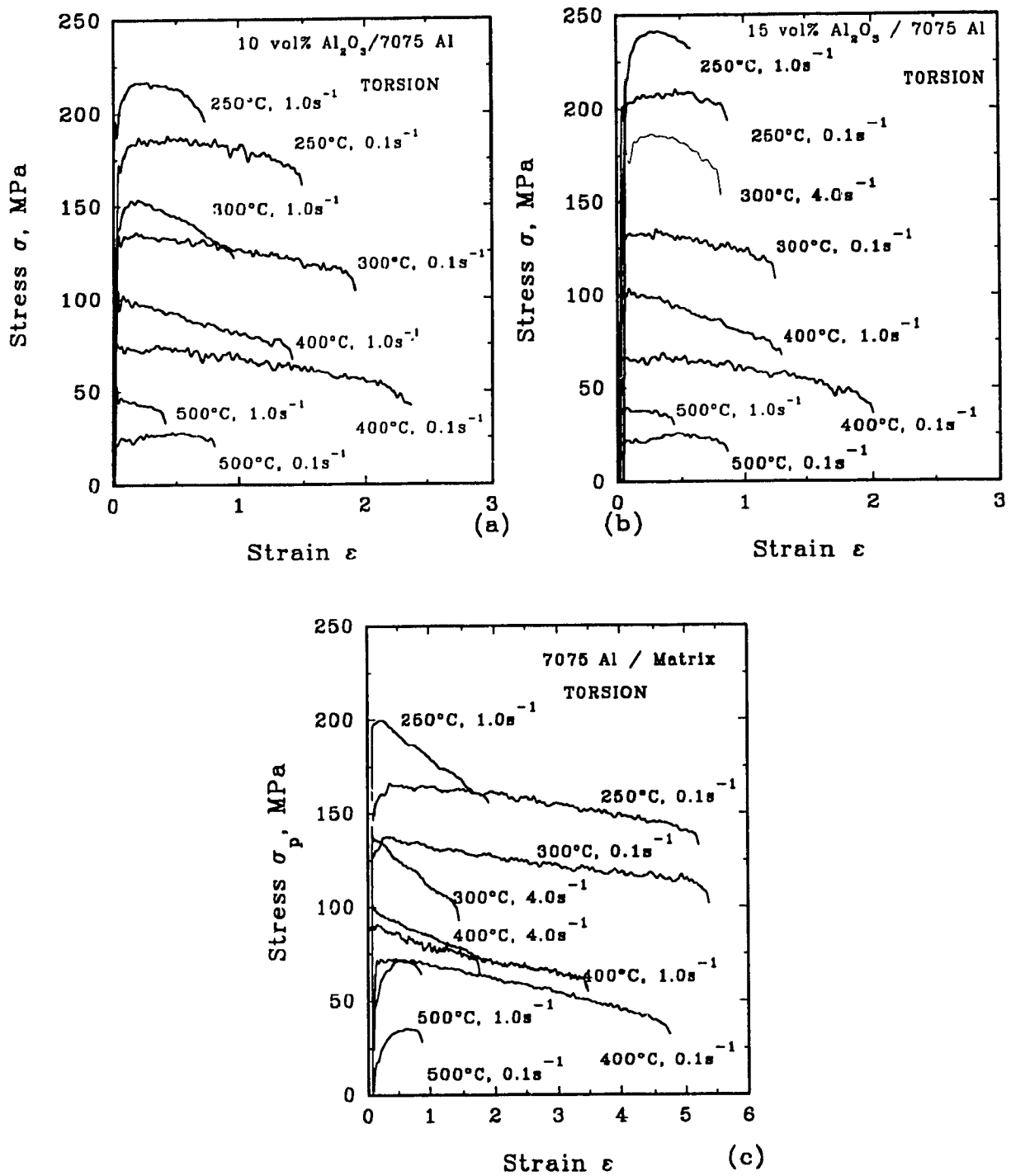
Figure 5.2   Representative σ-ε curves for: (a) 10% Al₂O₃/707 Al, (b) 15% Al₂O₃/7075 Al, (c) 7075 matrix alloy. The steady state stress rises with rising ε or declining T.

at lower temperatures. Although distinct peak stresses are seen in the flow curves especially for both composites, which may indicate dynamic recrystallization(DRX), the flow softening is considered to result from dynamic precipitation and coalescence, accompanied by some deformation heating; there is more of the latter at 250°C than at 400 ,or 500°C. There is also the possibility of the initiation of cracking in the material.

The flow stress declined monotonically as the deformation temperature rose for all three materials as illustrated in Figure 5.3. The composites are much stronger than the matrix alloy and the 15% Al_2O_3/7075 Al is stronger than the 10% Al_2O_3/7075 Al, particularly at the low temperatures. At 500°C, the difference of flow stress is only slight and the flow stress does not diminish very rapidly at high temperatures Table 5 1 lists the peak flow stress for three materials and the ratios for two composites with their matrix alloy, which further confirm the conditions of Figures 5.2 and 5.3.

5.1.2 Ductility

In the torsion test, the number of turns to fracture represents the ductility of a material. In Figure 5.2, the end of each flow curve exhibits the fracture strain ε_f which is plotted versus test temperature for the three materials(Figure 5 4). Generally, ductility increases with decreasing strain rate and increasing temperature as seen in Table 5 2, which lists the fracture strains at all test conditions. The fracture strain(ε_f) of the 10% Al_2O_3/ 7075 Al rose to a maximum of about 2.4 at 400°C for $\dot{\varepsilon}$=0.1 s^{-1}, whereas the 15% Al_2O_3/7075 Al reached a maximum of 2.0 at the same temperature and strain rate Compared to the matrix alloy, which has a high fracture strain of 4.0 at the same testing

Table 5.1   Peak flow stresses σ_p(MPa) and ratios obtained during hot working

Materials	$\dot{\varepsilon}$ (s^{-1})	250°C	300°C	400°C	500°C	540°C
A	0.1	187	136	76	28	12
B	0.1	207	155	67	27	10
C	0.1	165	120	72	36	
A	1.0	216	154	102	45	24
B	1.0	227	171	99	40	18
C	1.0	200	140	92	53	
A	4.0	222	160	115	59	23
B	4.0	242	187	120	59	25
C	4.0	197	143	106	50	

$\sigma_{AMC}/\sigma_{alloy}$

σ_A/σ_C	0.1	1.13	1.13	1.06	0.78
σ_B/σ_C	0.1	1.25	1.29	0.93	0.75
σ_A/σ_C	1.0	1.08	1.10	1.11	0.85
σ_B/σ_C	1.0	1.14	1.22	1.08	0.75
σ_A/σ_C	4.0	1.13	1.12	1.08	1.18
σ_B/σ_C	4.0	1.23	1.31	1.13	1.18

A 10% Al_2O_3/7075 Al;   B. 15% Al_2O_3/7075 Al;   C: 7075 Al Matrix Alloy.

Figure 5.3   Strengths for: (a) 10% Al₂O₃/7075 Al, (b) 15% Al₂O₃/7075 Al, (c)
7075 Al matrix alloy decrease uniformly with rising T dropping to
low values near 500°C.
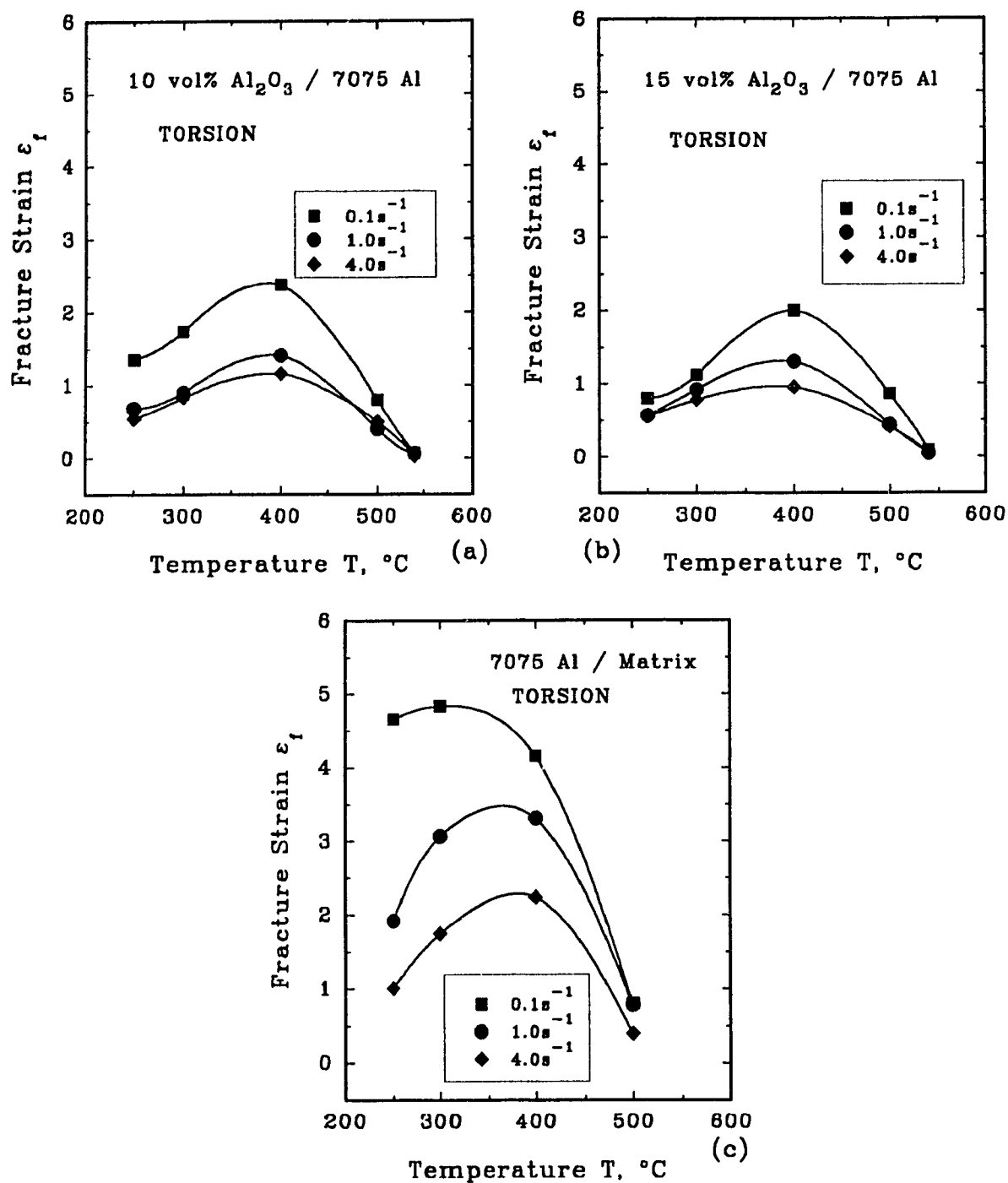
Figure 5.4   Ductilities for: (a) 10% Al$_2$O$_3$/7075 Al, (b) 15% Al$_2$O$_3$/7075 Al, (c) 7075 matrix alloy. Dependence of the ductility on temperature is shown at several strain rate.

Table 5.2   Fracture Strain ε_f obtained during hot torsion deformation

Material/$\dot{\varepsilon}$ s^{-1}	250°C	300°C	400°C	500°C	540°C
A / 0.1	1.35	1.74	2.38	0 80	0 07
A / 1.0	0.68	0.90	1.41	0 40	0 06
A / 4.0	0.54	0.83	1.16	0.50	0 03
B / 0.1	0.80	1.12	2.00	0.86	0.09
B / 1.0	0.56	0.92	1.30	0 44	0 05
B / 4.0	0.55	0.78	0.95	0.41	0.05
C / 0.1	4.66	4 84	4.16	0 80	
C / 1.0	1.92	3.07	3.07	0 79	
C / 4.0	1.01	1.75	1.75	0.40	

*   A: 10% Al$_2$O$_3$/7075 Al   B: 15% Al$_2$O$_3$/7075 Al   C: 7075 Al Matrix Alloy

condition, the torsional ductility of the two composites is about 50% less. Fracture strains for both composites increase until 400°C for all strain rates and decline as the temperature rises to 540°C. Unlike the composite material, 7075 matrix alloy displays a peak failure strain of 4.8 for 0.1 s^{-1} at 300°C.

5.1.3 Constitutive Plots

The dependence of flow stress on temperature and strain rate under hot working conditions can be analyzed and adequately described by Equation 3.4. The most suitable value of α is generally taken as the one that leads to the minimum standard deviation over the whole temperature range studied[81]. In the hyperbolic sine analysis, the optimum α should result in the constant temperature lines in plots of log $\dot{\varepsilon}$ versus log sinh $\alpha\sigma_p$ (Figure 5.5) being close to parallel However, in the present case, the value of α was selected as 0.052 MPa^{-1} from similar alloys as found in the literature; this facilitates the comparison of activation energy Q_{hw} and of data by graphical means. It can been seen from Figure 5.5 that the data are fitted reasonably well by approximately parallel straight lines with slopes n, each of which was derived by a least squares analysis. Figure 5.6 shows the relationship between log sinh $\alpha\sigma_p$ and 1/T; the slopes s of these constant $\dot{\varepsilon}$ lines were used to calculate the activation energies using the following equation:

$$Q_{hw} = 2.3nRs \qquad (5.1)$$

where s : slope of log sinh $\alpha\sigma_p$ versus 1000/T

First order regressions were performed on both the constant temperature and strain rate data to determine the values of the slopes n and s, respectively. The average of
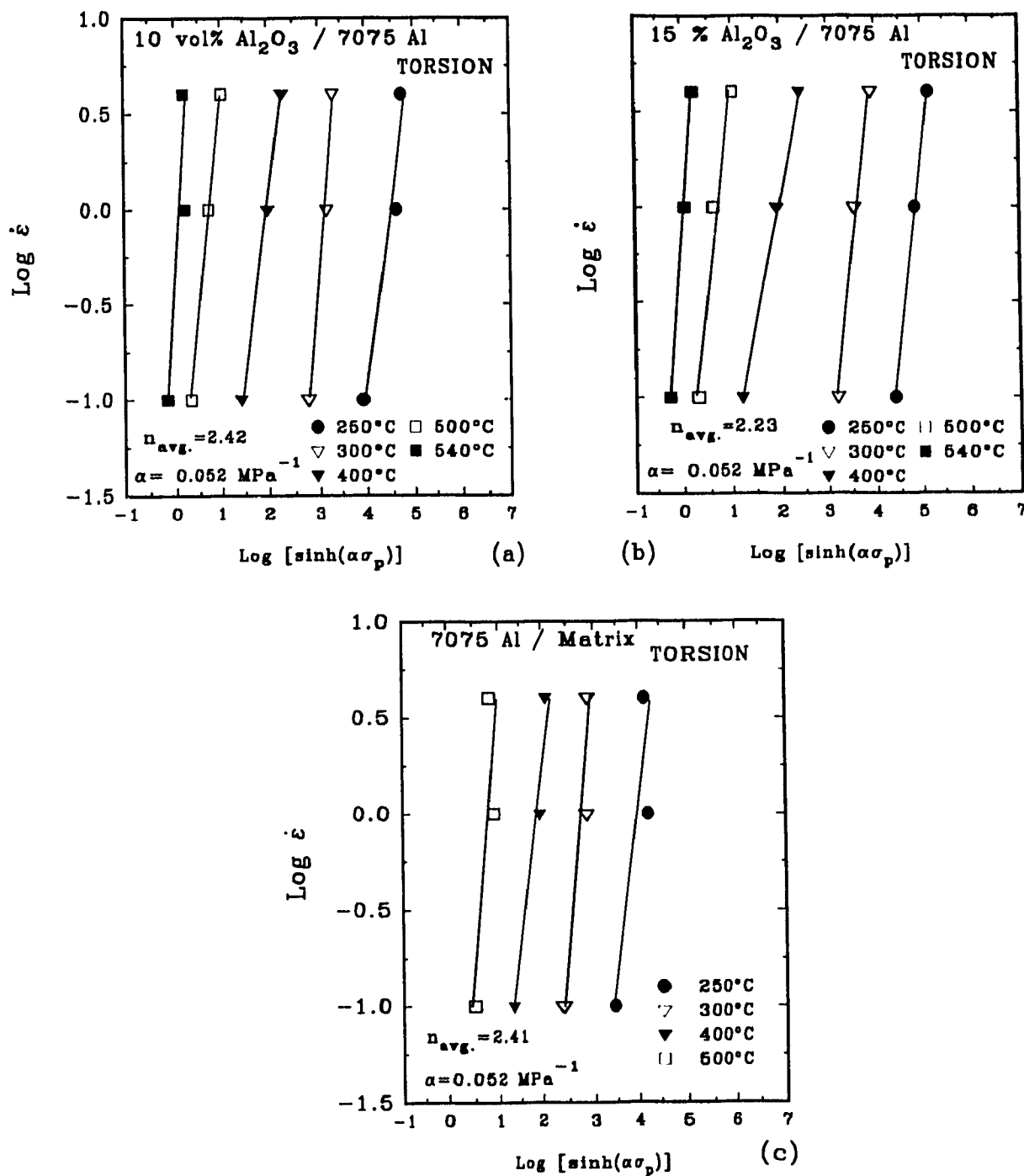
Figure 5.5   Plot of log ε̇ versus log sin ασ$_p$ (α=0.052 MPa[1]) for· (a) 10%
Al$_2$O$_3$/7075 Al, (b) 15% Al$_2$O$_3$/7075 Al, (c) 7075 Al matrix alloy
The linear behaviour supports the use of the sinh equation
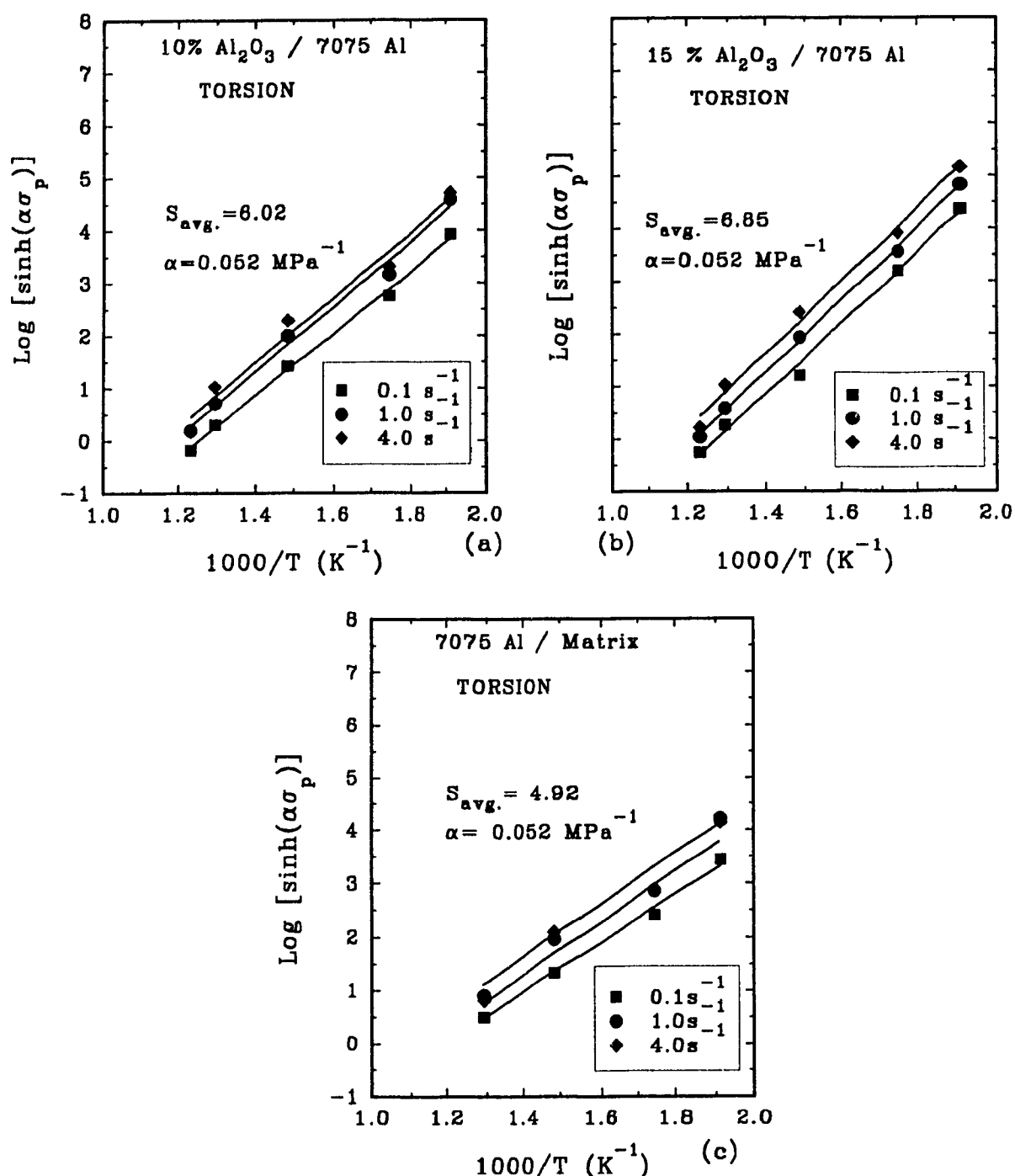
Figure5.6   Arrhenius relationship linking σ_p and T suit the data of: (a) 10% Al₂O₃/7075 Al, (b) 15% Al₂O₃/7075 Al, (c) 7075 Al matrix alloy indicating that straight lines can be drawn and a single Q_{HW} can be calculated.

n and s was calculated from the individual slopes which in turn were fitted back to the data as illustrated in Figures 5.5 and 5.6. It is apparent that these average slopes do not give the best fit lines especially at the low temperatures since the separations between some of the data points and the lines indicate experimental error. The values of n, s and Q_{HW} for each material are summarized in Table 5.3.

With progress in computational techniques, optimization of Equation 3.4 to fit the data is possible by selecting the most suitable combination of α, n and Q_{HW}. When there is a wide variety of α obtained, difficulty arises in finding any rational relationship between constitutive constants and the alloy composition. In the literature, there are often different values of α for the same material making comparable plots of log $\dot{\varepsilon}$ versus log sinh $\alpha\sigma_p$ difficult. To avoid this problem, in the present case, constitutive analysis was repeated with values of α which range from 0.01 to 0.10 MPa^{-1} to permit comparison for every material (Table 5.4). In order to show the distinct effects of varying α, the data plotted for 0.01, 0.02, 0.04, 0.052, 0.08 and 0.10 MPa^{-1}: both log $\dot{\varepsilon}$ versus log sinh $\alpha\sigma_p$ (Figure 5.7) and log sinh $\alpha\sigma_p$ versus 1000/T (Figure 5.8) for 10% Al_2O_3/7075 Al and Figures 5.9 and 5.10 for 15% Al_2O_3/7075 Al. In Figures 5.7 and 5.9, the sets of lines for increasing α values move to higher values of log sinh $\alpha\sigma_p$ and to lower n values. The linearity of the data for each temperature changes because the sinh function is not raised as a simple multiplier of rising α. A plot of n versus α (Figure 5.11) indicates that n decreases with rising α rapidly at first and then at a declining rate. Moreover in a plot against α, the slope s increases linearly as α rises but at a higher rate for higher strain rate (Figure 5.12)

Using Equation 5.1, Q_{HW} was calculated for all α values and appears in Table 5.4 Figure

Table 5.3   Summary of stress exponents($n_{avg.}$), slope($s_{avg.}$) and activation energies(Q_{HW}) for composites and their matrix alloy. (α=0.052 MPa^{-1})

Material	$n_{avg.}$	$s_{avg.}$	Q_{HW} (kJ/mol)
10% Al$_2$O$_3$/7075	2.42	6.02	279
15% Al$_2$O$_3$/7075	2.23	6.85	292
7075 Matrix Alloy	2.41	4.92	227

Table 5.4   Values of constants for various stress multipliers(α) for three materials.

10%Al$_2$O$_3$/7075 α (MPa^{-1})	n$_{avg.}$	S$_{avg.}$	A (s^{-1})	n$_z$	r	Q$_{nn}$ (kJ/mol)
0.01	7.64	1.75	$3.38*10^{20}$	7.09	0.9687	256
0.02	5.04	2.60	$2.49*10^{17}$	4 91	0 9873	251
0.04	3.04	4.70	$2.02*10^{17}$	3.00	0 9936	273
0.052	2.42	6.02	$2.31*10^{17}$	2 39	0.9941	279
0.08	1.71	9.18	$2.12*10^{18}$	1 69	0.9942	300
0.10	1.40	11.45	$3.79*10^{18}$	1.37	0 9941	306
15%Al$_2$O$_3$/7075 α(MPa^{-1})						
0.01	7.02	1.98	$1.69*10^{21}$	6.64	0.9750	266
0.02	4.45	2.96	$3.63*10^{17}$	4.39	0.9930	252
0.04	2.71	5.34	$6.27*10^{17}$	2.69	0.9975	277
0.052	2.23	6.85	$2.88*10^{18}$	2.21	0 9976	292
0.08	1.56	10.42	$2.20*10^{19}$	1.55	0.9973	311
0.10	1.28	13.00	$4.63*10^{19}$	1.27	0.9971	318
7075 Al/Matrix α(MPa^{-1})						
0.01	7.34	1.27	$1.03*10^{14}$	7.22	0.9828	178
0.02	5.56	2.01	$1.49*10^{14}$	5 45	0.9866	214
0.04	3.16	3.82	$1.14*10^{14}$	3.10	0.9886	231
0.052	2.41	4.92	$3.50*10^{13}$	2.35	0 9860	227
0.08	1.58	7.59	$1.55*10^{13}$	1.55	0.9860	230
0.10	1.28	9.51	$3.82*10^{13}$	1.25	0 9884	233
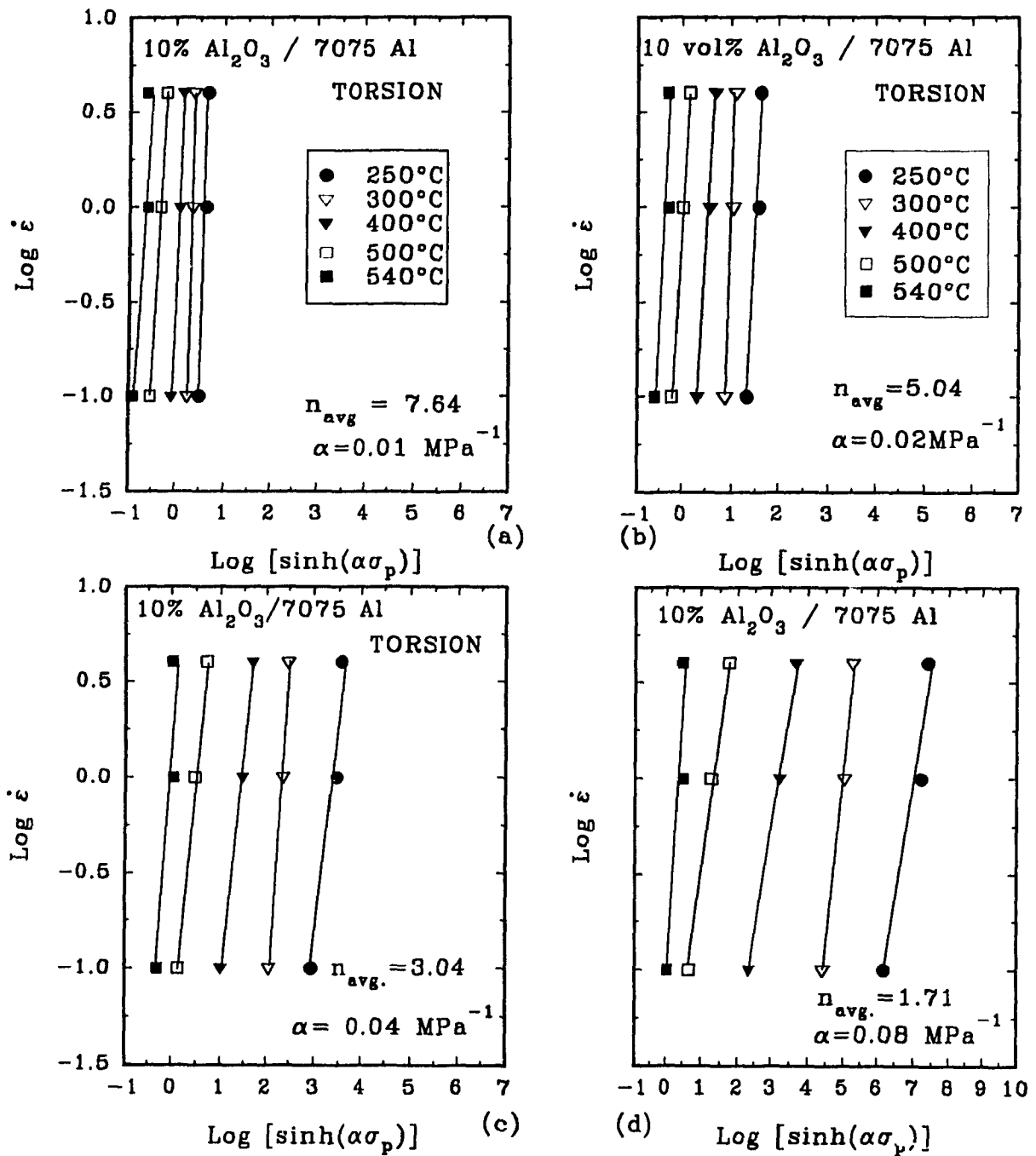
Figure 5.7   Plots of log ε̇ versus log sinh ασ_p for 10% Al₂O₃/7075 Al with: (a)
α=0.01MPa⁻¹, (b) α=0.02 MPa⁻¹, (c) α=0.04 MPa⁻¹, (d) α=0.08
MPa⁻¹ exhibit parallel lines for constant T which confirm Equation
3 4
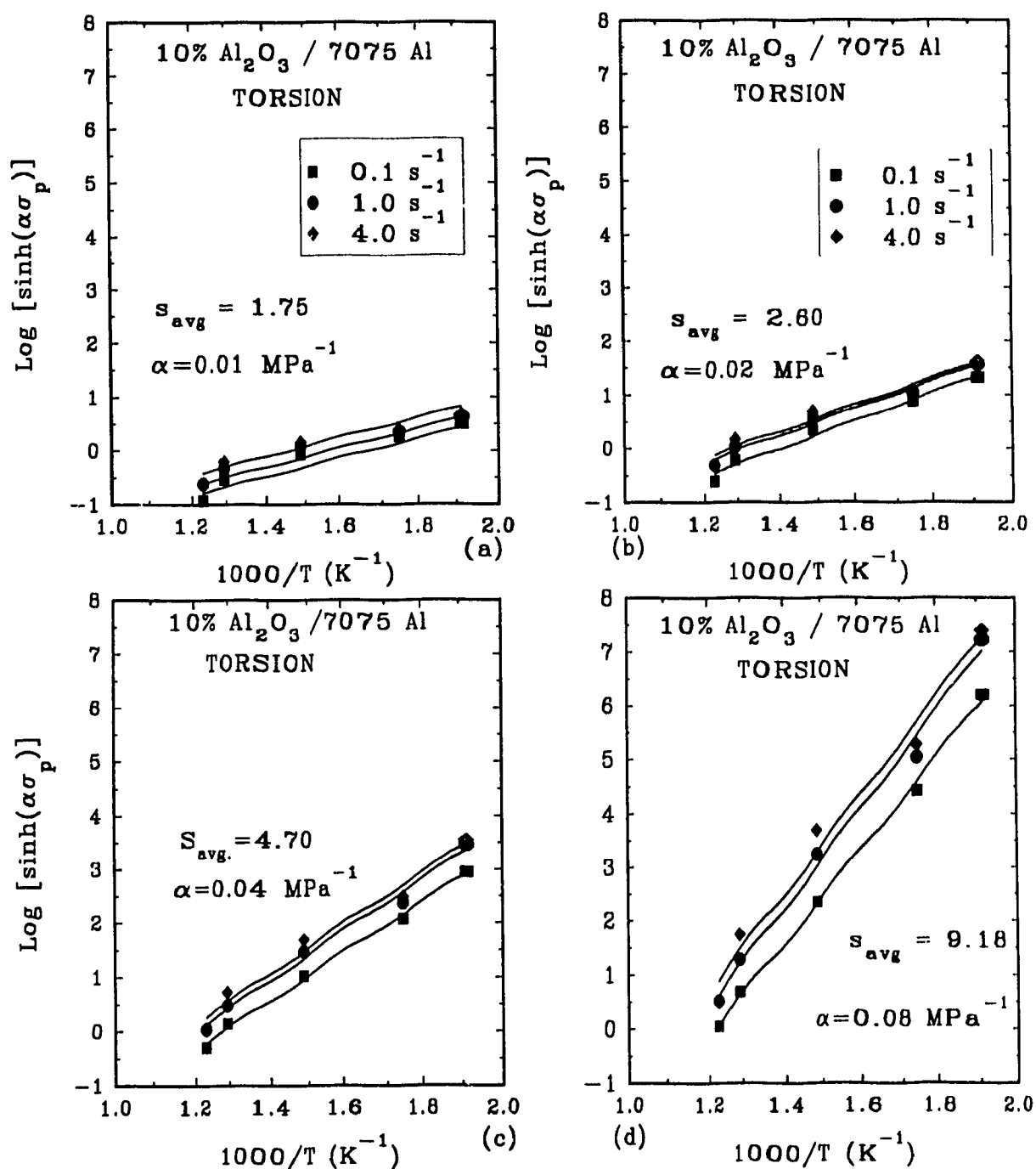
Figure 5.8   Arrhenius relationship linking σ_p and T is found for 10%
Al$_2$O$_3$/7075 Al: (a) α=0.01 MPa^{-1}, (b) α=0.02 MPa^{-1}, (c) α 0 04
MPa^{-1}, (d) α=0.08 MPa^{-1} according to Equation 3 4
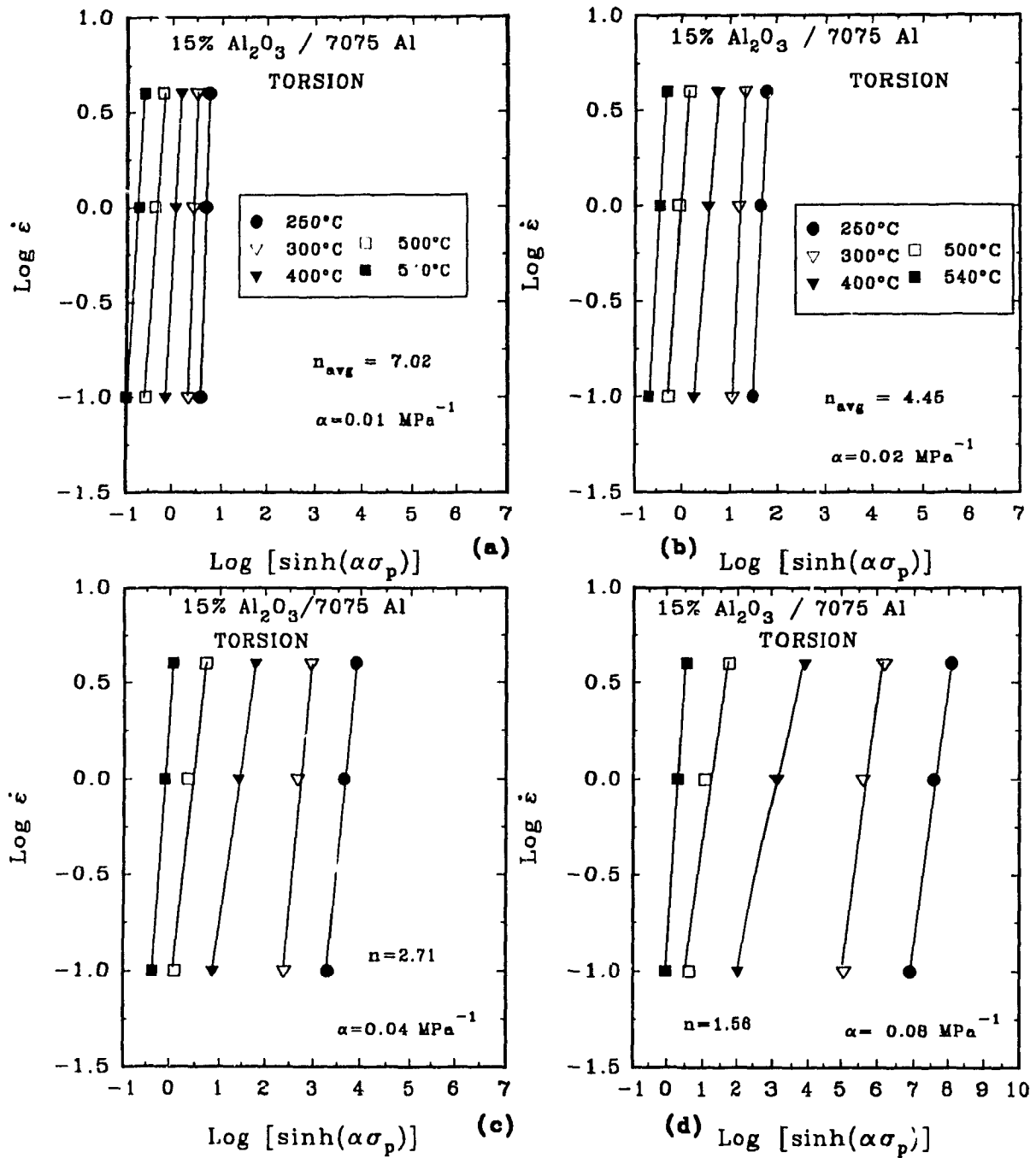
Figure 5 9   Plots of log ἐ versus log sinh ασ_p for 15% Al₂O₃/7075 Al with: (a)
α=0 01 MPa⁻¹, (b) α=0.02 MPa⁻¹, (c) α=0.04 MPa⁻¹, (d) α=0.08
MPa⁻¹ exhibit parallel lines for constant T which confirm Equation
3 4
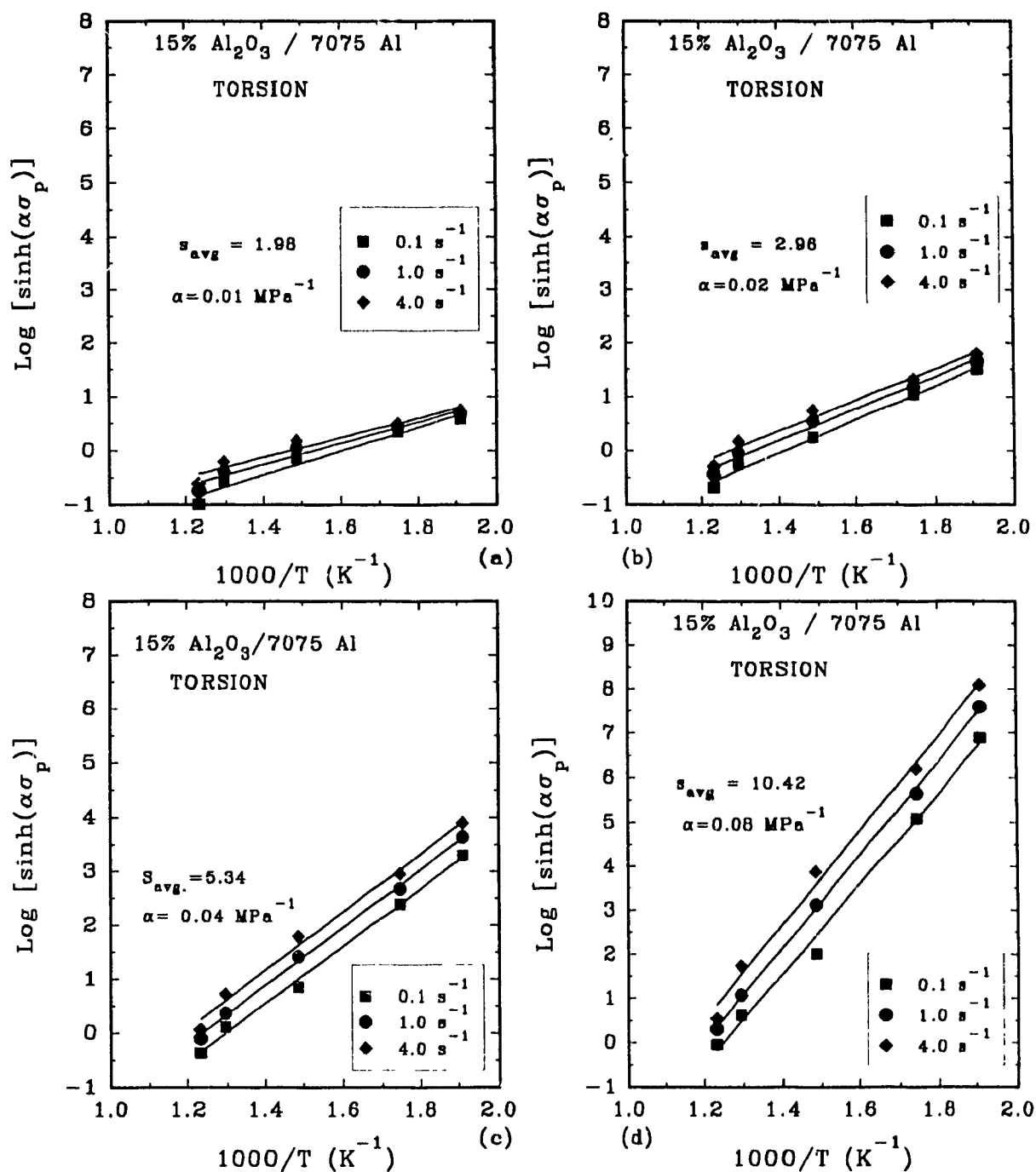
Figure 5.10   Arrhenius relationship linking σ and T is found for 15%
Al₂O₃/7075 Al: (a) α=0.01 MPa¹, (b) α=0.02 MPa¹,(c) α 0 04
MPa¹, (d) α=0.08 MPa⁻¹ according to Equation 3 4
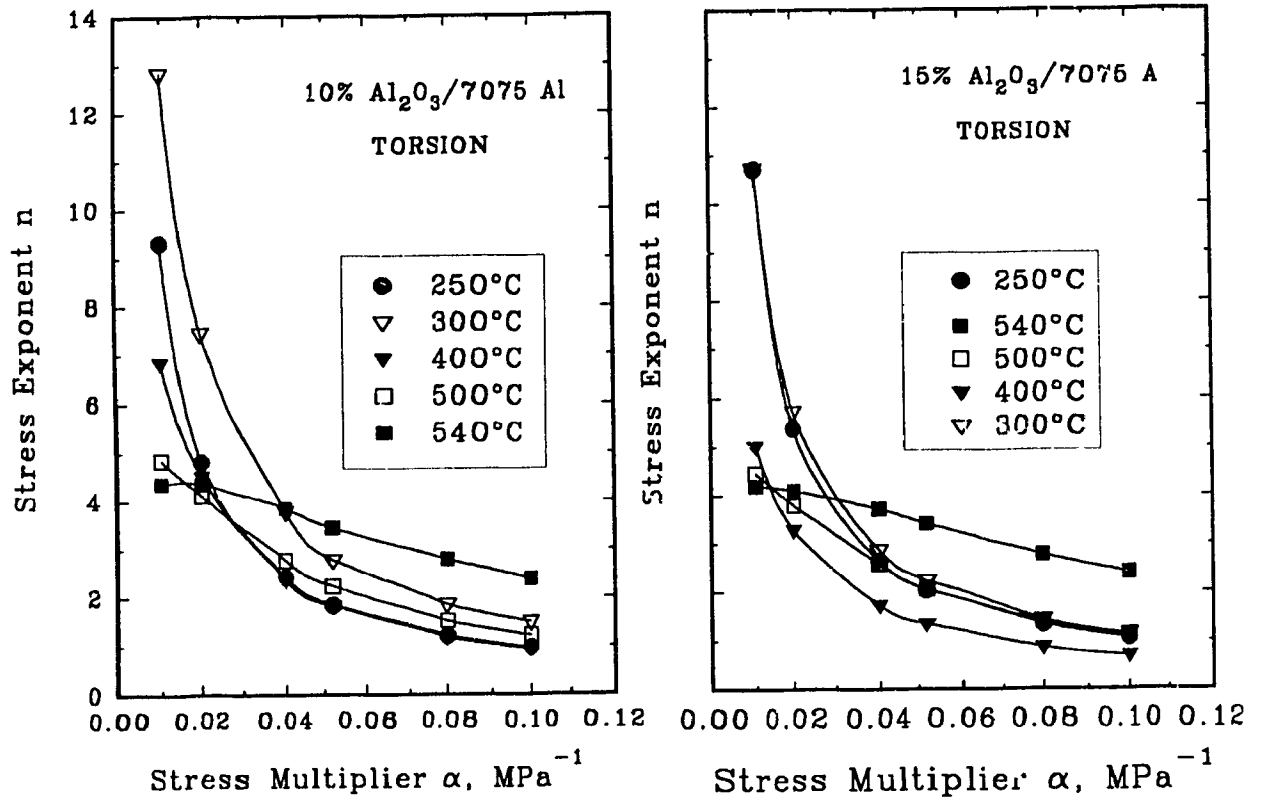
Figure 5 11   Plot of n versus α indicates that n declines at a diminishing rate as
α increases for 10% and 15% $Al_2O_3/7075$ Al.
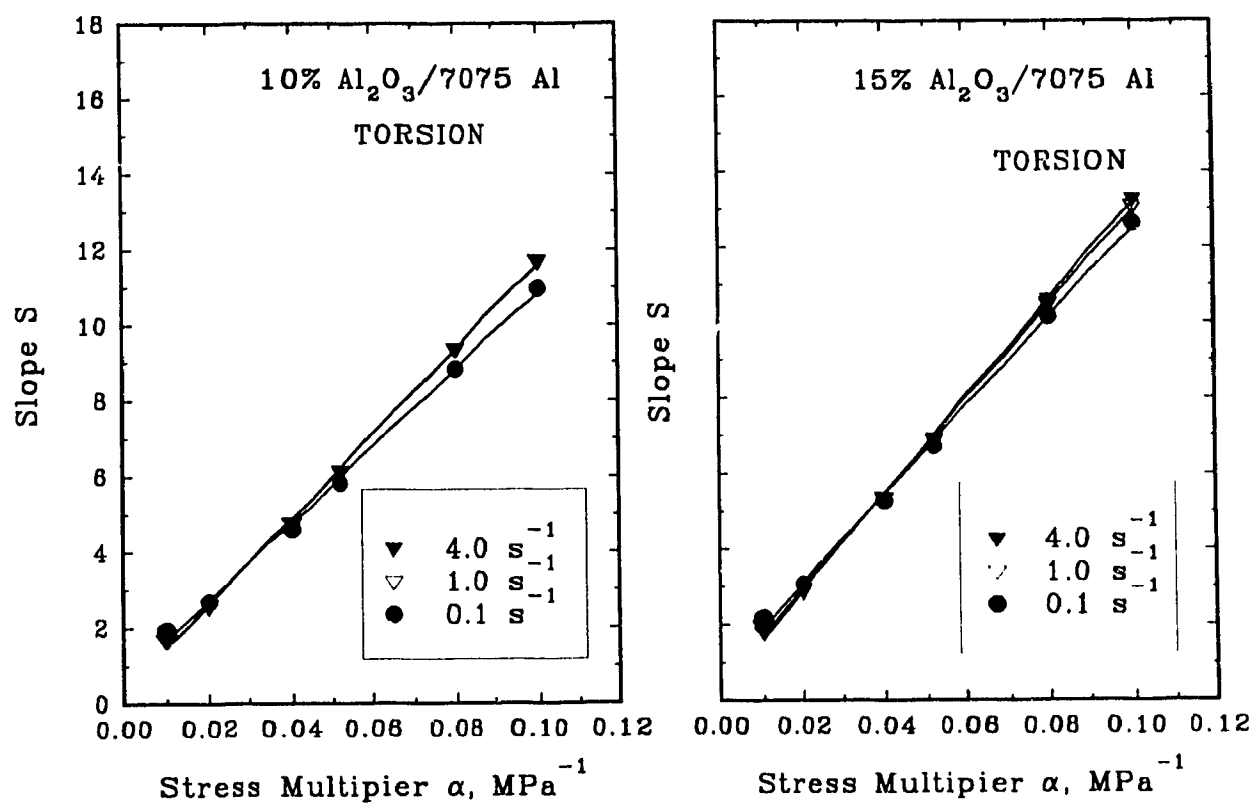
Figure 5.12   Plot of s versus α shows s increasing linearly as α rises but at a higher rate for higher ε
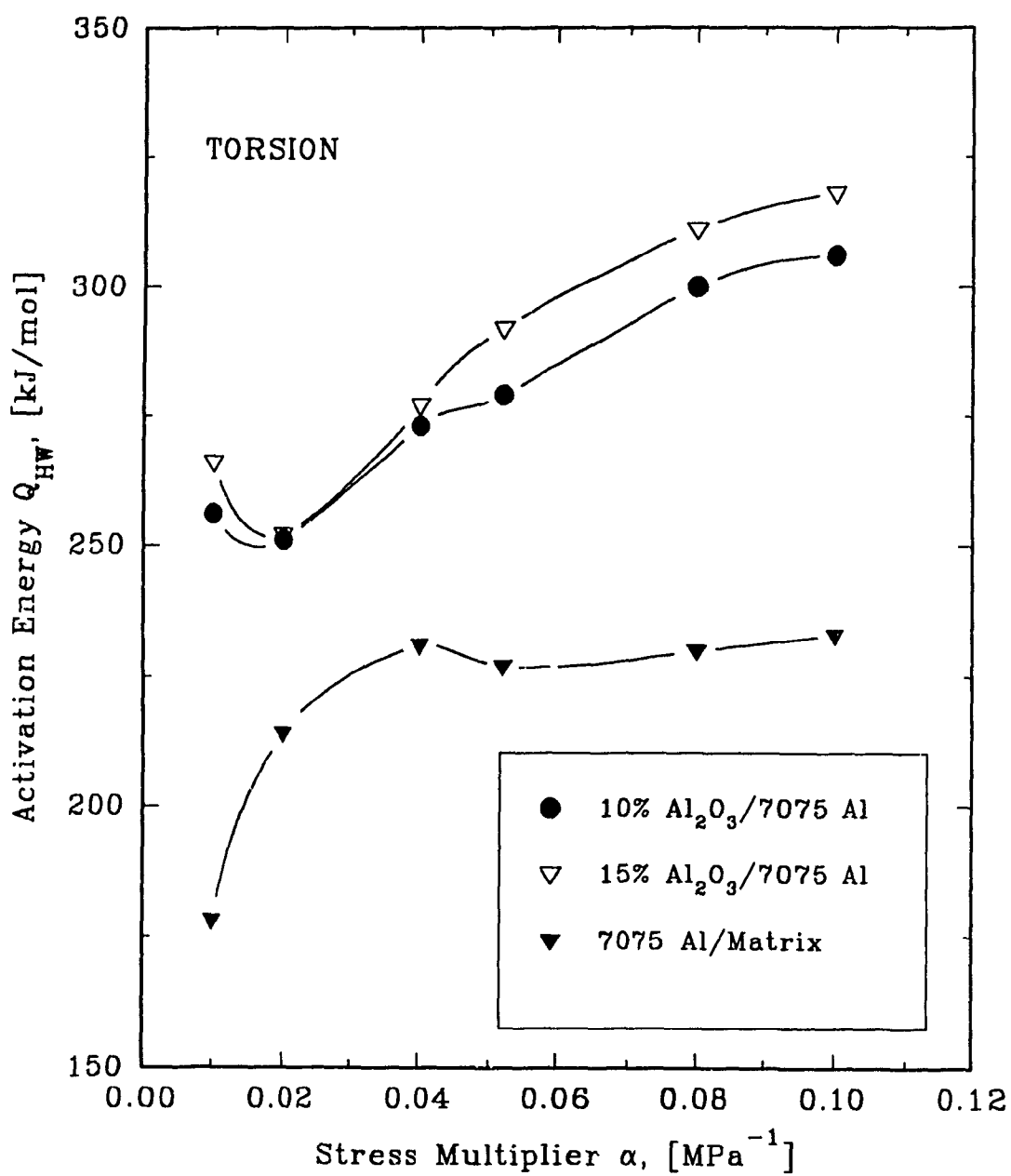
Figure 5 13   Activation energies Q_{HW} gradually increases with α increases.

5.13 shows Q_{HW} verses α, which as α increases, the value of Q_{HW} also increases. For the matrix alloy, the defference is getting smaller afer α=0 052 MPa ^{1}

With Q_{HW} determined, the combined effects of strain rate and temperature on the flow stress of the three materials can thus be described by Equation 3 4 It is possible to plot log Z against log sinh $\alpha\sigma_p$ in order to draw the data into single lines with slopes n and intercepts A as shown in Figure 5.14. It can be seen again that the flow stress increases as the deformation temperature is decreased and as the strain rate is increased. Figures 5 15, 5.16 and 5.17 show the plots of log Z vs log sinh $\alpha\sigma_p$ using different α values for 10% Al_2O_3/7075 Al, 15% Al_2O_3 / 7075 Al and 7075 Al matrix alloy.
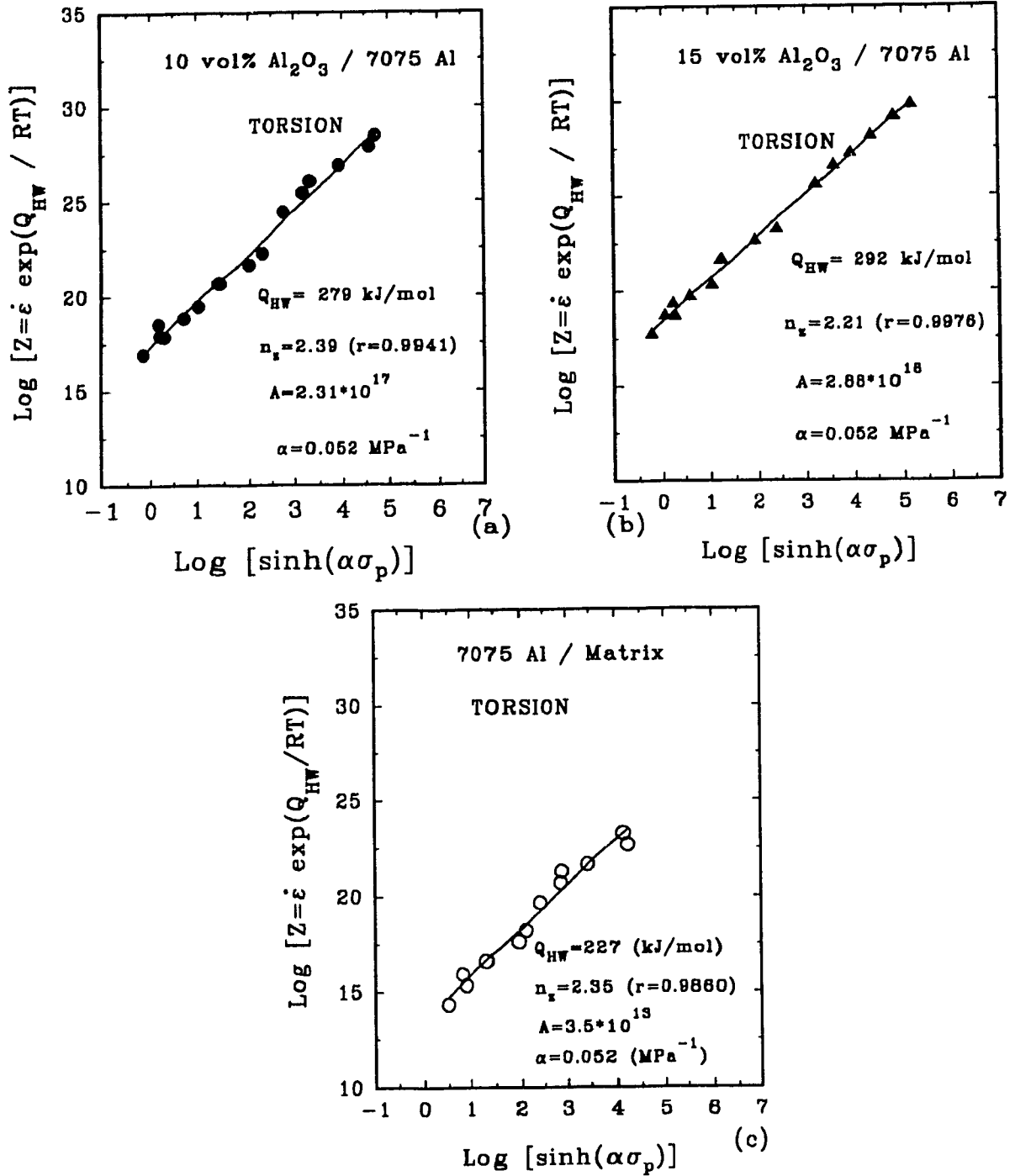
Figure 5.14   Through the use of the Z parameter, the data are organized into a single line:(a) 10% Al₂O₃/7075 Al,(b) 15% Al₂O₃/7075 Al (c)7075 Al matrix alloy for α=0.052 MPa⁻¹.
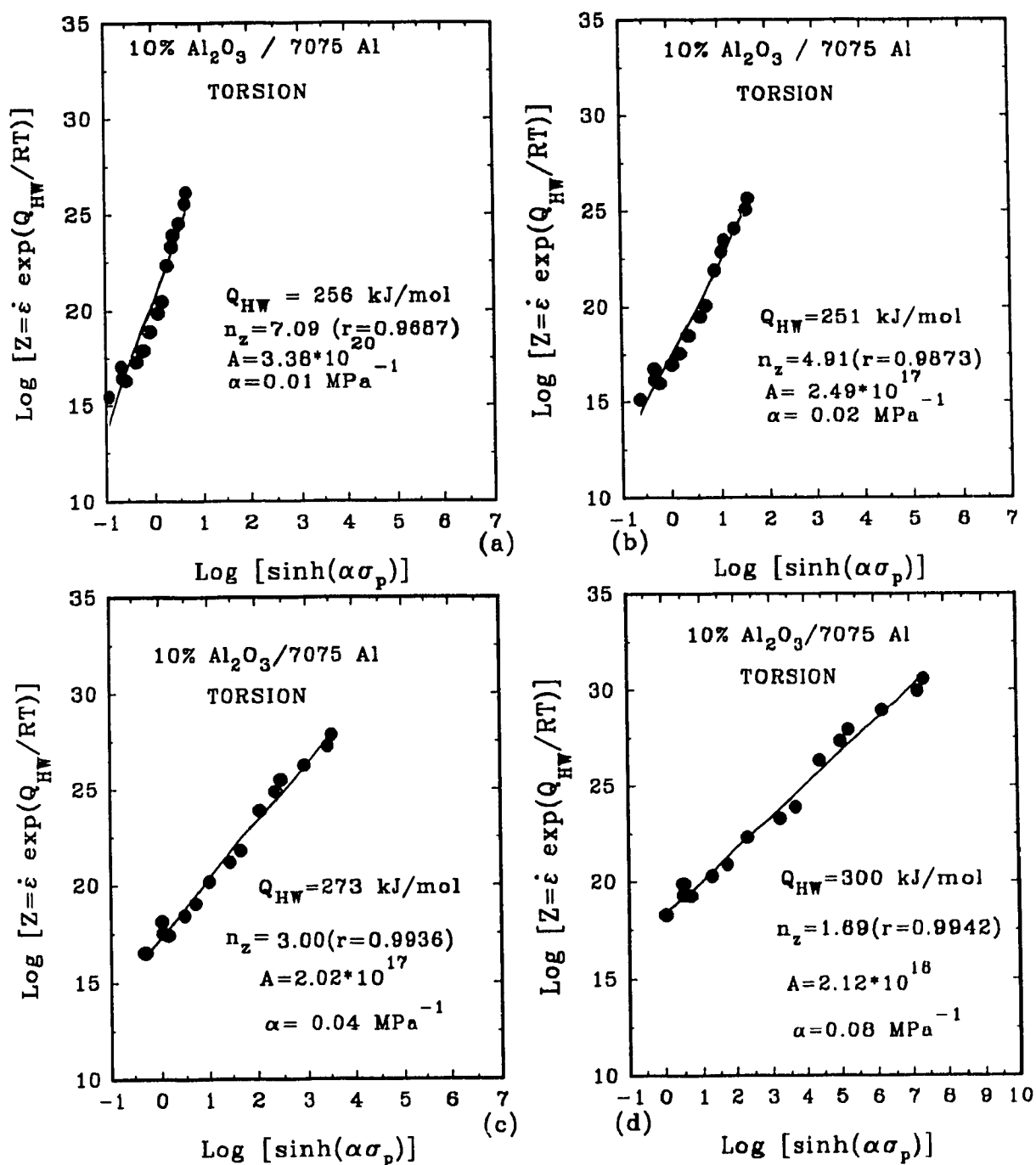
Figure 5.15   Dependence of composite flow stress on temperature and strain
rate through the Z parameter using different α values for 10%
Al_2O_3/7075 Al , (a) α=0 01 MPa', (b) α=0 02 MPa',(c) α 0 04
MPa⁻¹, (d) α=0.08 MPa⁻¹
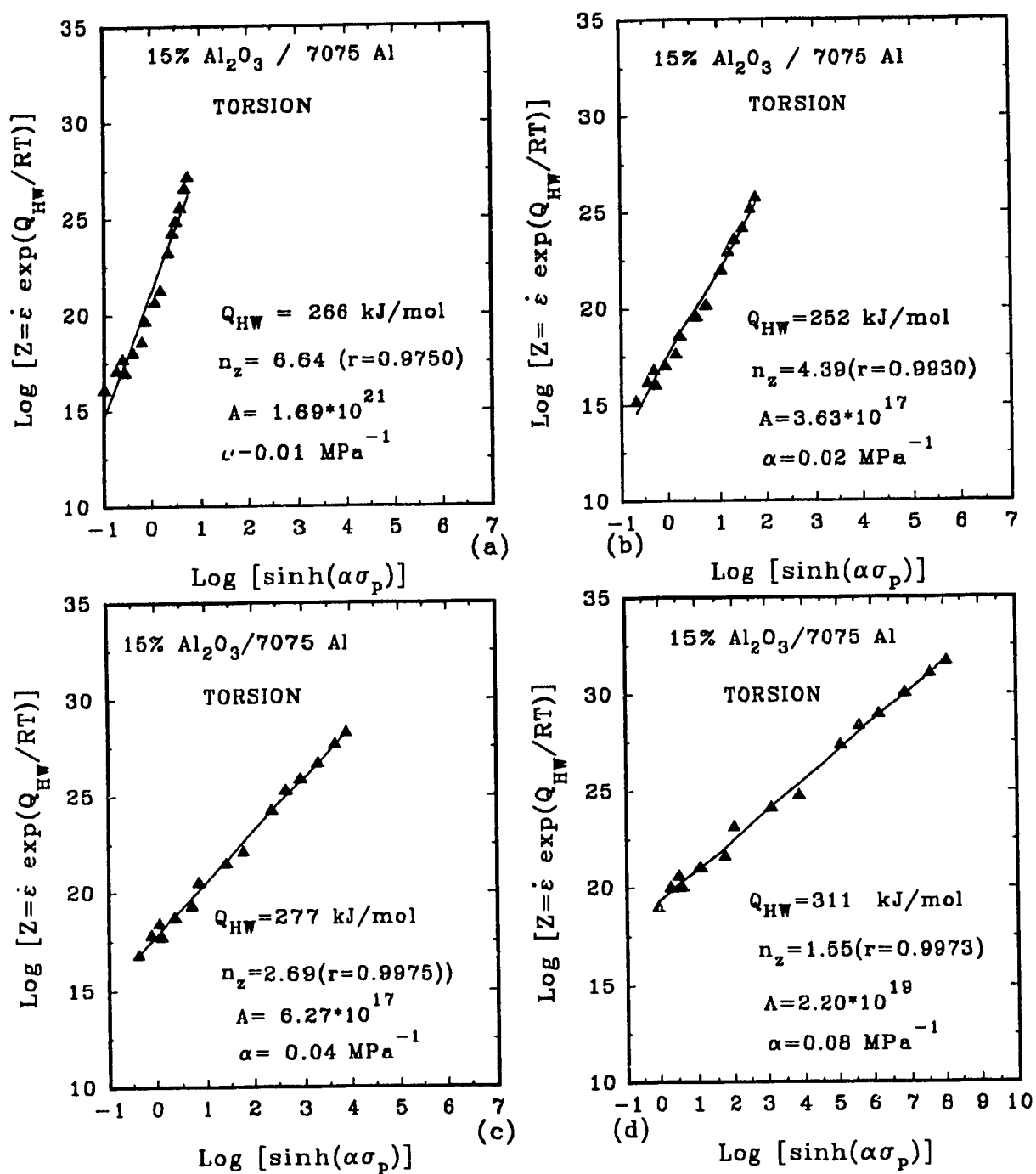
Figure 5.16   Dependence of composite flow stress on temperature and strain rate through the Z parameter using different α values for 15% Al_2O_3/7075 Al, (a) α=0.01 MPa^{-1}, (b) α=0.02 MPa^{-1},(c) α=0.04 MPa^{-1}, (d) α=0.08 MPa^{-1}
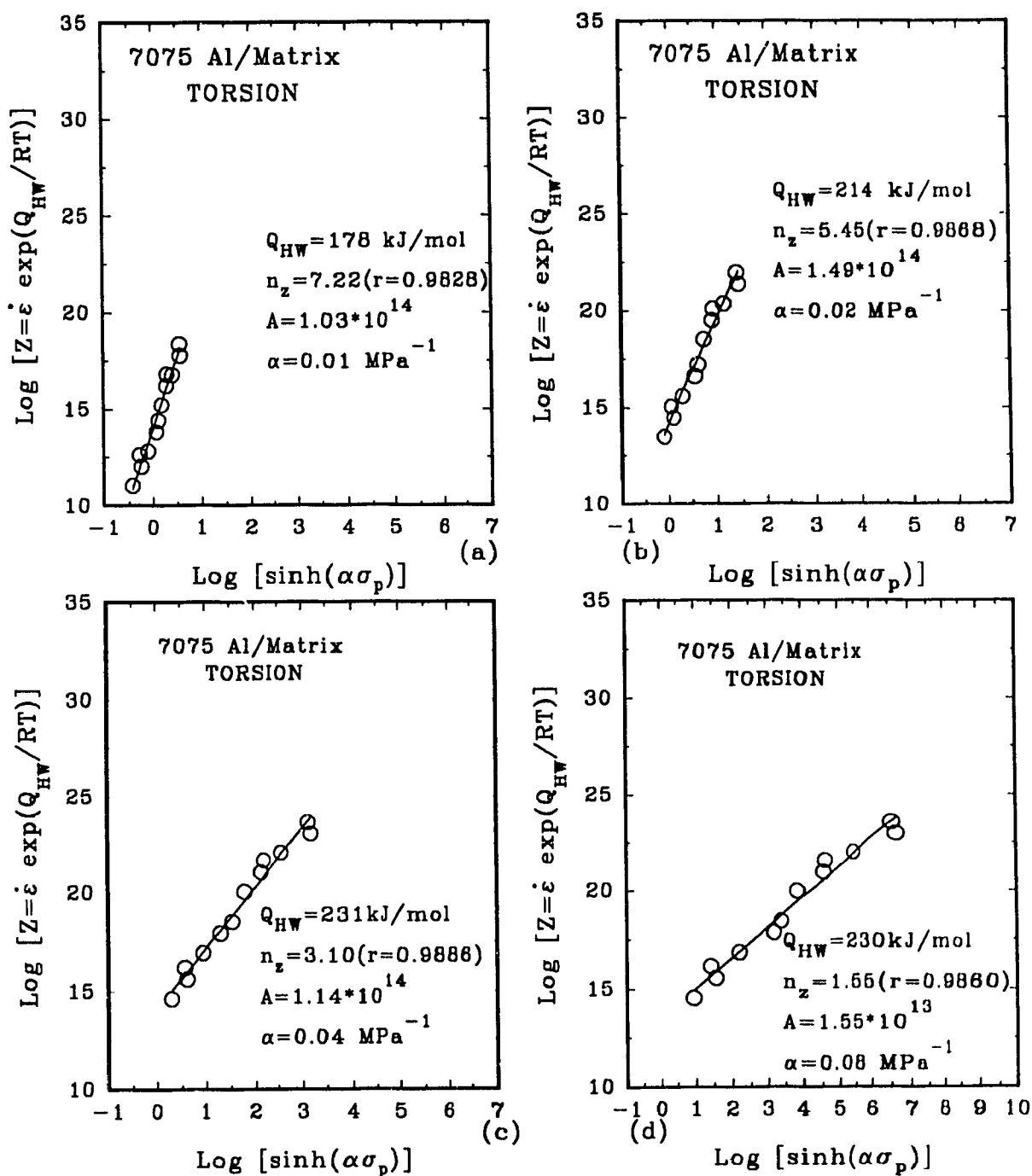
Figure 5.17   Dependence of composite flow stress on temperature and strain
rate through the Z parameter using different α values for
7075 Al matrix , (a) α=0.01 MPa⁻¹, (b) α=0.02 MPa⁻¹,(c)
α=0.04 MPa⁻¹, (d) α=0.08 MPa⁻¹

6. DISCUSSION

6.1 Continuous Deformation of Al_2O_3 / 7075 Al Composites and Its Matrix Alloy

It was found that both Al_2O_3 / 7075 Al and its matrix alloy display similar deformation characteristics when tested under identical deformation conditions. According to the theory of hot deformation, aluminum alloys undergo DRV to such an extent that they harden monotonically to a steady state regime which is much below ambient stress levels. Under these conditions, there is usually no peak in the stress-strain curve. An exception to this results from microstructural changes such as precipitate coarsening or from deformation heating. By contrast, a material which exhibits a peak in flow stress followed by considerable work softening to a steady state regime may be undergoing DRX. Although at and above 300°C initial peaks are followed by continual gradual softening for the composites and the matrix alloy (Figure 5.2), it is unlikely that DRX is the predominant restoration mechanism but rather DRV, since the latter has already been reported to be the principal softening mechanism in 7075 Al at high temperatures(75, 82) In Figure 5.2, the flow curve at 400°C displays decreasing flow stress, which may be associated with DRV accompanied by deformation heating, or perhaps by progressive fracture.

Research on a composite of 10% Al_2O_3/6061 confirmed that DRX occurred during hot working[83]. A high level of dislocation density shows limited DRV at 300°C As the test temperature rises, the dislocation density decreases and the sizes of the

subgrains/grains increase as DRV becomes more perfect, but never become as large as those in the alloy. Some of the 2μm dynamically recrystallized grains are formed around the 20μm Al_2O_3 particles; therefore particle stimulated DRX happened in 10%Al_2O_3/6061 Al composite.

In comparison to 10% Al_2O_3/6061 Al, 15% SiC_p/6061 Al composite has higher dislocation density, smaller subgrain/grain size, lower degree of dynamic recovery and more dynamically recrystallized nuclei[84]. In the work of Tuler et al.(13), DRX was observed in SiC_p / 6061 Al under hot compression conditions. A completely recrystallized structure was found in the 20% composite at 500°C, 5.0 s^{-1}, while recrystallization was just beginning in the vicinity of the SiC_p clusters in the 10% material. They concluded that DRX occurs through particle enhanced nucleation at the higher temperatures and strain rates. The above agree reasonably well with the view of Humphreys et al.(14) that particle enhanced nucleation is dependent on the volume percentage of particles and is likely in alloys with reduced recovery although not observed in a pure Al matrix at 425°C Determination of the substructure behavior of the Al_2O_3/7075 Al during softening and whether DRX occurs, will require electronic microscopic analysis.

As exhibited in Figure 5.3, 15% Al_2O_3 / 7075 Al is stronger than 10% / 7075 Al at 250 and 300°C; this difference in strength decreases as the temperature is increased The flow stresses increase with strain rate at all temperatures. Except at 540°C(Table 5 2), the two composites are stronger than the 7075 Al matrix alloy, which has maximum strengths of 130 and 80 MPa at 300 and 400°C (1.0 s^{-1}), respectively. The reasons for the observed difference in strength may be explained by means of a model of the dislocation

distributions as a function of T and $\dot{\varepsilon}$. In the test samples, there is a high, non-uniform density of the differential thermal expansion coefficient (ΔCTE) dislocations formed during cooling from solidification; there is also a complex distribution of internal stresses[69]. On heating to the deformation temperature, additional ΔCTE dislocations are generated around Al_2O_3 particles. Further more, for each particle considered separately, there is a highly localized flow in the adjacent matrix to make up for the absence of flow in the rigid particle. However, the effect of groups of particles must be considered; there are zones of high plastic flow between the particles. The plastic flow in hot working is affected by both the constraint for the rigid particles and from the initial distribution of ΔCTE dislocations which, moreover, varies with deformation T. While being thermally equilibrated at the deformation T, plastic flow relieves the internal stresses that are higher than the yield stress for that T. There is also static recovery of the substructure which is greater at higher T thus reducing the density more. In addition during deformation, DRV attempts to reduce the dislocation density and develop a substructure consistent with the local strain rate conditions[17, 18]. The 15% Al_2O_3 / 7075 Al composite has more ΔCTE dislocations and more plastic flow constraints than the 10% Al_2O_3 / 7075 Al composite, which can be responsible for the much greater strain hardening.

The suitability of the sinh-Arrhenius equation was to be expected, since it has been used for many other Al alloys[17, 18, 85, 86]. In previous reports on similar composite materials, both Tuler et al.[13] and Pickens et al.[11] chose to use the power law (Equation 3.2) in their analyses In Picken's research on 7090 +20% SiC and 6061 +20% SiC, ln σ vs ln $\dot{\varepsilon}$ was not a good linear fit at 400°C; and also ln σ vs 1/T was not linear,

indicating that the deformation process is too complex to be characterized by a single activation energy over the temperature range studied. However, using the sinh relationship, we determined that Arrhenius plot is linear(Figure 5.6) such that a single Q_{hw} can be calculated[7, 8].

To facilitate comparison, $\alpha = 0.052$ MPa^{-1} was initially employed The values of $Q_{hw}=279$ and 292 kJ/mol for 10% and 15% Al$_2$O$_3$ reinforced composites are considerably higher than that of the matrix alloy(227 kJ/mol). Usually the bulk alloys have Q_{hw} in the range 160-200 kJ/mol, which are higher than for commercial purity Al where 150 kJ/mol can be related to vacancy migration and dislocation climb. Compared to 6061 and A356 composites[78], Q_{hw}'s are in the range 180 and 260 kJ/mol A higher Q_{hw} value for 7075 composites can be attributed to high strengths at 300 and 250°C but the flow stresses are similar at 500°C; as a result, the s value increases, raising the activation energy The high activation energies, compared to that of the Al alloy indicate that DRV is impeded by complex interactions between dislocations, particles and solute[87] Industrially, a higher Q_{hw} indicates that in a conventional rolling schedule with declining T, the finishing passes will require higher force.

The high activation energies observed in the composites can be explained by the model of the substructure development. At high T, the AMC flow stresses are almost the same as those for the bulk alloy because the DRV mechanisms and limited DRX are able to reduce the dislocation densities to about the same level, despite the non-uniform strain distribution imposed by the rigid particles As T decreases, the initial dislocation density is higher and more heterogeneous. The strain distribution due to the particles tends to

become less uniform because of the higher yield stress and localized T increases in the high shear regions. In comparison to the bulk alloy, it becomes more difficult for the DRV mechanisms to rearrange the dislocations into orderly, low energy arrays in association with annihilations: it is to be emphasized that the rates of the unit mechanisms such as climb are not changed, it is just that they do not accomplish as much In the bulk alloy for any condition, the substructure reaches an equilibrium state related to the flux of dislocations defined by $\dot{\varepsilon}$ and the ability of the unit mechanisms to eliminate and rearrange dislocations[17, 18]. In the composites at low T, the equilibrium is never reached as indicated by absence of a steady state regime.

In age hardenable Al alloys deformed in the solution treated condition, there are increasing levels of dynamic precipitation as T declines leading to very high initial stresses[17]. However, as strain progresses, the particles coalesce and recovery is able to reduce the initial high dislocation density to develop a steady state at the same level as material overaged prior to deformation. The activation energies of the overaged matrix alloys are similar to that for pure Al[17, 18]. The higher stresses at low T in 7075 Al matrix composite, compared to 6061 Al matrix composite, may be related to higher levels of precipitation in the former

The effects of α variation on n and s are to be expected from the nature of the $\sinh(\alpha\sigma_p)$ function(Figures 5 11 and 5.12). The decrease at declining rate for n and the linear increase for s agree with results for other alloys[88]. The initial rapid change and final saturation for Q_{hw} for the alloy is in agreement with a previous analysis, which led to the recommendation that α should be in the range 0.04 to 0.08 MPa^{1} in order to facilitate

comparison of activation energies between different alloys[88]. The composites only saturated in the rang 0.08 to 0.10 MPa^{-1}(Figures 5.15 and 5.16).

The ductilities of the two composites increase with temperature in the range 250-400°C. The ductility of the 10% Al$_2$O$_3$ / 7075 Al composite is higher than that of the 15% Al$_2$O$_3$ / 7075; the maximum fracture strains(ε_f) at 400°C reach 2.4 and 2.0, respectively With fracture strains of 4.8 and 4.3 observed at 300 and 400°C for the 7075 bulk alloy, the workability of the composite can be considered quite good However, the ε_f of the two composites and the alloy declined substantially when the temperature was raised over 400°C, and became similar for different strain rate conditions. So that the decline at higher T's may be interpreted as a result of low matrix ductility. This phenomena is similar with that of Picken's research on 7090 with 20% SiC reinforcement and its matrix alloy[11]. It was found that ε_f for the 7090 composite passed through a maximum value of 0.6 at a deformation temperature of 427°C, whereas the 7090 Al passed through a much higher maximum of 2.3 at about 288°C before declining to similar values above 400°C.

The much lower ductility(ε_f) of the composites than that of the bulk matrix alloy below 400°C is mainly related to the higher dislocation density, which arises from reduced DRV in the matrix and which induces stress concentration at the reinforcing particle/matrix interfaces[14] This may cause debonding during hot deformation and initiation of cracks which link up and lead to an earlier fracture. The ε_f values of AMC generally exhibit only a slight increase for diminishing strain rate conditions unlike the matrix alloys Moreover ε_f decreases with increase in the reinforcing particle volume fraction.

6.2 Industrial Applications

About 80% of total metal and alloy production involves hot working. Difficulties such as insufficient ductility at low temperatures or high strain rates have been solved by empirical techniques mainly through the reduction of certain impurities and the specification of working limits. A major goal has been to determine a functional relationship between the parameters so that the flow stress and forming forces can be predicted for any condition which often involves a complex pattern of temperature, strain rate and strain. Such information on new materials is extremely valuable in assuring that the processing operation will not exceed the capacity of the equipment. In materials developed for high strength, hot ductility is often a problem so it is necessary to know how it varies with temperature and strain rate.

DURALCAN aluminum composites combine the light weight and strength attributes of aluminum with the stiffness and wear resistance of ceramics to create a material offering unique properties to various engineering fields (automotive, industrial, commercial and recreational). These composites also offer low thermal expansion and excellent thermal conductivity. Generally alloys made with ceramic powder are difficult to hot work because the high flow stress leads to extremely high extrusion breakout pressures. In addition, they often have limited hot ductility which can manifest itself as surface break-up during extrusion or cracking during forging or rolling. Studies to improve the hot working behavior of metal matrix composites are difficult to perform for several reasons. Experimental material is extremely expensive and consequently it is often

not practical to hot work many billets over a wide range of conditions to optimize hot working parameters. Fortunately, such hot working studies can be performed using relatively small test specimens on hot working simulators such as the hot torsion machine Hot torsion testing has been successfully used to simulate extrusion and predict the maximum allowable extrusion ratio and also to generate microstructures that correspond to those produced during extrusion In addition, hot torsion testing has been used 'o optimize hot rolling parameters for commercial aluminum alloys. Utilization of torsion testing with its wide range of capabilities could uncover formability schedules which might not be found through less flexible testing techniques[78].

7. CONCLUSIONS

- The flow stresses decrease uniformly with increasing deformation temperature for both the composites and their matrix alloy The flow stress for 15% Al_2O_3/7075 Al is generally higher than that for 10% Al_2O_3/7075 Al, but the difference is quite small at higher temperature. Flow stresses for the composites rise more rapidly than their matrix alloy with increasing strain rate.

- The torsional ductility of 10% Al_2O_3/7075 Al is slightly higher than that of the 15% vol. material; both reach a peak value at 400°C The ductilities for both composites decrease rapidly above 400°C. The ductility of either composite is only 50% that of the matrix alloy at 400°C but similar at 500°C. The composites have high dislocation density which leads to high stress concentrations in the metal matrix at the reinforcing particles which bring about crack initiation The high stress also enhances cracking at grain boundaries.

- The plots of log $\dot{\varepsilon}$ versus log sinh $\alpha\sigma_p$ are linear over the range of strain rate tested with slopes that are fairly independent of temperature for α=0 052 MPa^{-1}, which gives the best correlation. The stress exponents(n) for 10% Al_2O_3/7075 Al and 15% Al_2O_3/7075 Al were calculated to be 2.42 and 2.23, respectively The Arrhenius plots were also linear, showing that the activation energies for both the 15% Al_2O_3/7075 Al (Q_{hw} 292 kJ/mol) and the 10% Al_2O_3/7075 Al (Q_{hw}= 279 kJ/mol) composites were higher than their matrix alloys (Q_{hw} = 227 kJ/mol).

- Due to similarity of mechanical behavior with 6061 composite, we may expect that the particles increase the average dislocation density more with rising volume fraction

- The optimum value of the stress multiplier for the composites was determined to be in the range of 0.04 to 0.08MPa^{-1} from the view point of highest correlation However, from the view point of almost constant $Q_{ IIW}$ value, 0.08 to 0.10 MPa^{-1} would be better. For the matrix alloy, the two criteria give the same range from 0.04 to 0.08 MPa^{-1}.

REFERENCES

[1] John V. Foltz and Charles, "Metal-Matrix Composites", **Metals Handbook**, vol 2, eds. Joseph R Davis, et al., ASM International, 1990, pp 903-912

[2] S. Abis, "Characteristics of an Aluminium Alloy/Alumina Metal Matrix Composite", **Composites Science and Technology**. 35, 1989, pp 1-11

[3] R. J. Arsenault and Y Flom, "Role of interfaces in SiC/Al Composites", **Proceedings Of A Symposium On Structure And Deformation Of Boundaries**, OCT 13-17, 1985 Toronto ONT, Canada, pp 261-279

[4] D J. Lloyd, "Particulate Reinforced Composites Produced by Molten Metal Mixing", **High Performance Composites For The 1990's**, eds S K Das, et al, Warrendale, PA: TMS-AIME, 1991, pp.33-45.

[5] D. J. Lloyed, "Metal Matrix Composite-An Overview", **Advanced Structural Materials**. ed. D. S.Wilkinson, Oxford, UK: Pergamon Press, 1989, pp 1-21

[6] D J Lloyed, "The Solidification Microstructure of Particulate Reinforced Aluminum/SiC Composites", **Composites Science & Technology**, 35, 1989, pp 159-179.

[7] H. J. McQueen and P Sakaris, "Mechanical Shaping of Metal Matrix Composites", **Composite Structures and Materials**, eds S. V Hoa and R Gauvin, Elsevier Applied Science, London, 1992, pp.297-306

[8]   P Sakaris and H J McQueen, "Hot Workability of SiCp/6061 Al Composites".

        Aluminum Alloys: Their Physical and Mechanical Properties, ICCA3, ed. L.

        Arnberg et al., Vol. 1, Trondheim, Norway: NTH-SINTEFF, 1992, pp.554-559

[9]   F J. Humphreys, "Deformation and Annealing Mechanisms in Discontinuously

        Reinforced Metal-Matrix Composites", **Mechanical and Physical Behaviour of**

        Metallic and Ceramic Composites, ed. S. I. Andersen, et al., Roskilde,

        Denmark: RISO Natnl. Lab., 1988, pp.51-74.

[10]   W. C Harrigan Jr , G. Gaebler, E. G. Davis and E. J. Levin, "The Effects of Hot

        Rolling on the Mechanical Properties of SiC-Reinforced 6061 Aluminum",

        Mechanical Behaviour of Metal Matrix Composites, ed. J. E. Hack, et al ,

        Warrendale, PA:TMS-AIME, 1983, pp.169-180.

[11]   J R Pickens, T J. Langan, R. O. England and M. R. Liebson, "A Study of the

        Hot Working Behaviour of SiC-Al Alloy Composites and Their Matrix Alloys by

        Hot Torsion Testing", **Metallurgical Transactions A**, 18A, 1987, pp.303-312.

[12]   Z. Xiong, L. Geng and C. K. Yao, "Investigation of High-Temperature

        Deformation Behaviour of a SiC Whisker Reinforced 6061 Aluminum

        Composite", **Composites Science and Technology**, 39, 1990, pp.117-125.

[13]   F. R Tuler, J. T. Beals, C. Demetry and D. Zhao, "Deformation Mechanism

        Mapping of SiC/Al Metal Matrix Composites Materials", **Cast Reinforced Metal**

        Composites, ed. S. G. Fishman, et al., Materials Park, OH: ASM, Intnl., 1988,

        pp.321-325.

[14]   F. J. Humphreys, W. S Miller and M. R Djazeb, "Microstructural Development

During Thermomechanical Processing of Particulate Metal Matrix Composites",

Materials Science & Technology, vol 6, 1990, pp.1157-1166

[15]   P. Sakaris and H. J. McQueen, "Comparative Hot Workability of SiCp/A356 and

SiCp/6061 Al Composites and their Matrices", **Metal Matrix Composites,**

Fabrication and Technology, Edmonton, Conf. Montreal, CIMM, 1992

[16]   E. Evangelista, A. Forcellese and F.Gabrielli, "Hot Working Behaviour of

Whiskers Reinforced SiC/Al Composite", **Processing and Properties of**

Materials, Birmingham IRC, 1992.

[17]   H. J. McQueen and K. Conrod, "Recovery and Recrystallization in the Hot

Working of Al Alloys", **Microstructural Control in Aluminum Alloy**

Processing,   ed. E. H. Chia and H. J. McQueen, Warrendale, PA: TMS-AIME,

1986, pp.197- 220.

[18]   H. J. McQueen, "Micromechanisms of Dynamic Softening in Aluminum Alloys

During Hot Working", **Hot Deformation of Aluminum Alloys**, ed. T. G

Langdon, et al., Warrendale, PA: TMS-AIME, 1991, pp.31-54.

[19]   H. J. McQueen, "Effect of Solutes and Precipitates on Hot Working Behaviour of

Al Alloys", **Hot Deformation of Aluminum Alloys**, ed. T G. Langdon, et al ,

Warrendale, PA: TMS-AIME, 1991, pp.105-120.

[20]   H. J. McQueen and J. J. Jonas, "Recent Advances in Hot Working Dynamic

Softening Mechanisms", **J. Applied Metalworking**, 8, 1984, pp.235-241

[21] H. J McQueen and J J. Jonas, "Role of Dynamic and Static Softening in Multistage Hot Working", ibid, pp.410-420.

[22] F. J. Humphreys and P. N. Kalu, "Dislocation Particle Interactions During Hot Deformation of Al Alloys", **Acta Metallurgica**, 35, 1987, pp.2815-2829.

[23] K. P. Rao, S. M. Doraivelu, H. Md. Roshan and Y. V. R. K. Prasad,"Deformation Processing of an Aluminum Alloy Containing Particles: Studies on Al-5Pct Si Alloy 4043", **Metallurgical Transactions A**, 14A(1983), pp.1671-1679.

[24] M. Hunt, "Making Metal Matrix Composites Stronger and Tougher", **Materials Engineering**, July 1989, pp.44-46.

[25] M Hunt, "Aluminum Composites Come of Age", **Materials Engineering**, January 1989, pp 37-40.

[26] N Gane, "Developments in Powder Metallurgy", **Materials Forum**, vol. 13, 1989, pp.81-100.

[27] Huda, "Compaction Behaviour of Metal Matrix Composite", Paper pesented at the IMF-8 92, University College, Dnblin, 15 Sept. 1992.

[28] T. Sritharan, K. Xia, J. Heathcock and J. Mihelich, "Matrix/Reinforcement Development for Aluminum-Based Composites", **Meral & Ceramic Matrix Composites: Processing, Modeling & Mechanical Behavior**, eds. R. B. Bhagat, et al., The Minerals, Metals & Materials Society, 1990, pp.13-22.

[29] A. Mortensen, "Interface Chemistry of Inorganic Composite Materials", **Proc. 9th Riso International Symposium on Metallurgy and Materials Science**. ed. S Andersen et al., 1988, pp.144-155.

[30]   A. H. Heuer, L. U. Ogbuji and T. E. Mitchell, "The Microstructure of Oxide

        Scales on Oxidised Si and SiC Single Crystals", **Journal of American Ceramic**

        Society, 63, 1980, pp.354-355.

[31]   J. L. Cook and W. R. Mohn, "Whisker-Reinforced MMCs", **Engineered**

        Materials Handbook, vol. 1, Composites, ASM International, Metals Park, Ohio,

        1987, pp.896-902.

[32]   M. Hunt, "Automotive MMCs: Better and Cheaper", **Materials Engineering**,

        October 1989, pp.45-47.

[33]   D. Charles, "Metal Matrix Composites-Ready for Take Off", **Metals and**

        Materials, February 1990, pp.78-82.

[34]   B. J. Maclean and M. S. Misra, "SiC-Reinforced Aluminum Alloys for Aerospace

        Applications", **Mechanical Behaviour of Metal Matrix Composites**, The

        Metallurgical Society of AIME, Warrendale, PA, 1983, pp 301-320

[35]   D. Huda, M. A. El Baradie and M. S. J. Hashmi, "Manufacture and

        Characterization of Aluminium Matrix Composite Using Powder Metallurgy

        Route", **Advanced Composites'93**, eds. T. Chandra et al., pp.1029-1035

[36]   A. K. Dhingra, "Alumina Fibre FP", **Philos. Trans. R. Soc. London A**,

        vol.294, 1980, pp.411-417.

[37]   A. K. Dhingra, "Advances in Inorganic Fiber Developments", **in Contemporary**

        Topics in Polymer Science, vol 5, E. J. Vandenberg, Ed., Plenum Press, 1984,

        pp.227-260.

[38] Y Abe, K Fujimura, and S. Horikira, "Review: Alumina Fibers and Composite

Materials", **J. Japan. Soc. Compos. Mater.**, vol 6, No.3, 1980, pp.89-97

[39] J D. Birchall,"The Preparation and Properties of Polycrystalline Aluminium

Oxide Fibres", **in Fabrication Science**, vol 3, No.33, ed. D. Taylor, The British

Ceramic Society, 1983, pp.51-62.

[40] J. Dinwoodie, E Moore, C. A. J. Langman, and W. R. Symes, "The Properties

and Applications of Short Staple Alumina Fibre Reinforced Aluminum Alloys",

Conference Proceedings of the Fifth International Conference on Composite

Materials, July/Aug 1985, pp 671-685.

[41a] Gerald L. DePoorter, Terrence K. Brog and Michael J. Readey, "Structural

Ceramics", **Metals Handbook**, vol. 2, ASM International, 1990, pp.1019-1024.

[42] C G. Levi, G J Abbaschian and R. Mehrabian, "Interface Interactions During

Fabrication of Aluminium Alloy-Aluminium Fiber Composite", **Metallurgical**

Transactions 9A, 1978, pp.687-711.

[43] A. Munikz, M. Metzgen and R. Mehrabian, "The Interface Phase in Al-

Mg/Al_2O_3", **Metallurgical Transaction 10A**, 1979, pp.1491-1497.

[44] D. O Karlsen et al., "Transmission Electron Microscope Study of the Interface

Region in Al Matrix Composites", **Proc. 9th Riso International Symposium on**

Metallurgy and Materials Science, ed. S. Audersen, et al., 1988, pp.421-425.

[45] I. W. Hall and V. Barrailler, "The Effect of Thermal Exposure on the

Microstructure and Fiber/Matrix Interface of an Al_2O_3/Al Composite",

Metall. Trans., 17A, 1986, pp.1075-1080.

[46]   A K. Dhingra and W. H. Krueger, "New Engineering Material-Magnesium

Castings Reinforced With Continuous Alumina Fiber FP", **in Proceedings of the**

36th World Confference on Magnesium, International Magnesium Association,

1979.

[47]   M. G. Bader, T. W. Clyne, G. R. Cappleman, and P. A Hubert, "The Fabrication

and Properties of Metal-Matrix Composites Based on Aluminum Alloy Infiltrated

Alumina Fibre Preforms", **Compos. Sci. Technol.**, vol 23, 1885, pp 287-301

[48]   A. Mortensen, M. N. Gungor, J. A. Cornie and M. C Flemings, "Alloy

Microstructures in Cast Metal Matrix Composites", **J. Met.**, March 1986, pp 30-

35

[49]   C. G. Levi, G. J. Abbaschian and R. Mehrabian, "Interface Interactions During

Fabrication of Aluminum Alloy-Alumina Fiber Composites", **Metall. Trans. A**,

vol 9A, 1978, pp.697-711.

[50]   J. E. Hack, R. A. Page and R. Sherman, "The Influence of Thermal Exposure on

Interfacial Reactions and Strength in Aluminum Oxide Fiber Reinforced

Magnesium Alloy Composites", **Metall. Trans. A**, vol 16A, 1985, pp 2069-2072

[51]   W. R. Hoover, "The Commercialization of Aluminum Composites", **Advanced**

Composite'93, ed. T. Chandra, et al., The Minerals, Metals and Materials

Society, 1993, pp.957-961.

[52]   S. Lal and G. S. Upadhyaya, "Sintering of Stainless Steel and Their Based

Composites", **Rev. Powder Metall. and Physical Ceramics**, 3(2), 1986, pp 165-

203.

[53]   Y L Liu, "Microstructure, Texture and Mechanical Properties of Al-SiC$_w$ Composites Manufactured by Powder Blending", **Proc. of the 1989 Powder Metallurgy Conference and Exhibition**, San Diego, USA, June 11-14, 1989, vol 3, pp.461-474.

[54]   F. Kloucek and R. F. Singer, "Properties of Short Fiber Reinforced Aluminum Alloys", **Proc. of Advanced Materials Research and Developments for Transport Composite 1985**, Nov. 26-28, France, 1985, pp.249-256.

[55]   Milton W. Toaz, "Discontinuous Ceramic Fiber MMCs", **Composites**, vol. 1, ASM International, 1987, pp.903-910

[56]   W. C. Harrigan Jr., "Discontinuous Silicon Fiber MMCs", **Engineered Materials Handbook**, vol. 1, **Composites**, ASM International, Metals Park, Ohio, 1987, pp 889-895.

[57]   M. A. Bayoumi, H Ribes and M. Suery, "Aging Characteristics of SiC-Particle Reinforced Al-SiC Alloys", **Mechanical and Physical Behaviour of Metallic and Ceramic Composites**, 9th RISO International Symposium on Metallurgy and Materials Science, 1988, pp.291-296.

[58]   Jack W. Bray, "Aluminum Mill and Engineered Wrought Products", **Metals Handbook,** vol 2, eds. Joseph R. Davis et al.. ASM International, 1990, pp.29-61

[59]   J. K. Shang and R.O.Ritchie, "On the Particle Size Dependence of Fatigue Crack Propagation Thresholds in SiC Particulate Reinforced Aluminum Alloy Composites", **Acta Metallurgica**, 37, 1989, pp.2267-2278.

[60]   J. J. Lewandowski, C. Liu and W. H Hunt, "Effect of Matrix Microstructure and
        Particle Distribution on Fracture of on Aluminum Metal Matrix Composite",
        Materials Science and Engineering A107, 1989, pp 241-255.

[61]   H. J. McQueen, **Hot Deformation of Aluminum Alloys, TMS-AIME**, eds T. G
        Longdon, et al., Warrendale, PA, 1991, pp.105-116.

[62]   H. J.   McQueen, W. A. Wong and J. J. Jonas, "Deformation of Aluminum at
        High Temperature and Strain Rates", **Canadian Journal of Physics**, vol 45,
        1967, pp.1225-1234.

[63]   H. J. McQueen and W. J. M. Tegart, "The Deformation of Metals at High
        Temperatures", **Scientific American**, vol. 232, no. 4, April 1975, pp 116-124

[64]   R. A. Petkovic, M. J. Luton, and J. J. Jonas, "Recovery and Recrystallization of
        Carbon Steel Between Intervals of Hot Working", **Canadian Metallurgical
        Quarterly**, vol. 14, no.2, 1975, pp.137-145.

[65]   H. J. McQueen, "Deformation Mechanisms in Hot Working", **Journal of Metals**,
        vol. 18, no. 4, April 1968, pp.31-38.

[66]   H. J. McQueen, "Dynamic Recovery and Its Relation to Other Restoration
        Mechanisms", **Metallurgia I Odlewnictwo**, vol. 5, no. 3, 1979, pp 421-451.

[67]   H. J. McQueen, E. Evangelista, M. E. Kassner, "The Classification and
        Determination of Restoration Mechanisms in Hot Working of Al Alloys",
        Zeitschrift fur Metallkunde, vol. 82, no. 5, 1991, pp.336-345

[68]   J. J. Jonas, H. J. McQueen and W. A. Wong, "Deformation under Hot Working
        Conditions", (SP 108), **Iron Steel Inst**., London, 1968, pp.49-59.

[69]   R. J. Arsenault, **Strength of Metals and Alloys, ICSMA 9**, Tel-Aviv, eds. D. G.
        Brandon, et al., Freund Pub. Co. Ltd., London, U. K., 1990, pp.31-46.

[70]   K. Kannikeswaran and R. Y. Lin, "Trace Elements Effect on Al-SiC Interfaces",
        Journal of Metals, 1987, pp.17-19.

[71]   H. J. McQueen, "Review of Simulations of Multistage Hot-Forming of Steels",
        Canadian Metallurgical Quarterly, vol 21, No. 4, 1982, pp.445-460.

[72]   W. J. McG. Tegart, **Elements of Mechanical Metallurgy**, New York: The
        MacMillan Company, 1969, pp 37-38.

[73]   Norman Daniel Ryan, "Work Hardening, Strength, Restorative Mechanisms, and
        Ductility in the Hot Working of 300 Series Stainless Steels", Ph.D. Thesis,
        Concordia University, Montreal, 1989.

[74]   P. Sakaris and H. J. McQueen, "Hot Workability of 6201 Al Alloy", **Aluminum
        Alloys: Their Physical and Mechanical Properties**, ICAA3, vol. 2, Trondheim,
        1992, pp.276-281.

[75]   E. Evangelista, A. Forcellese, F. Gabrielli and P. Mengucci, "Hot Workability of
        Some Heat Treatable Aluminum Alloys",**Hot Deformation of Aluminum Alloys,**
        TMS-AIME, Warrendale, PA, 1991, pp.121-139.

[76]   D.S.Fields and W.A.Backofen, Proc. ASTM. 57, 1957, p1259.

[77]   S. Fulop, K. Cadien, M. J. Luton, H. J. McQueen, "A Servo-Controlled Hydraulic
        Torsion Machine for Hot Working Studies", **Journal of Testing and Evaluation**,
        vol. 5, 1977, pp.419-426.

[78]   Peter Sakaris, "Hot Deformation Behavior of SiCp/Al Composites and Their

        Materices and an Al-Mg-Si Alloy", **Master Thesis**, Concordia University,

        Montreal, 1993.

[79]   S. L. Semiatin, G. D. Lahoti and J. J. Jonas, "Application of Torsion Test to

        Determine Workability", **Metals Handbook**, vol. 8, 9th ed , Ohio, American

        Society for Metals, 1985, pp.154-184.

[80]   T. M. Maccagon, S. Yue, J. J. Jonas and K. Dyck, "Simulated Hot Working, Cold

        Working, and Annealing of Al-Containing Steels", **Metall. Trans. A**, vol 24A,

        July 1993, pp.1589-1596.

[81]   D.Yu and T. Chandra, "Effect of Temperature and Strain Rate on Flow Behaviour

        and Microstructure in 6061 Aluminum Containing Al_2O_3 Particles", **Advanced

        Composites'93**, eds. T. Chandra et al., 1993, pp.1073-1077.

[82]   E. Evangelista, E. Di Russo, H. J. McQueen and P. Mengucci, **Homogenization

        and Annealing of Aluminum and Copper Alloys**, eds. H.D. Merchant et al.,

        1988, p.209.

[83]   X. Xia, H. J. McQueen and P. Sakaris, "Deformation and Microstructure of Al_2O_3

        Particle Reinforced 6061 Al Composite", **Developments and Applications of

        Ceramics and New Metal Alloys**, eds. R. A. L. Drew and H Mostaghaci, August

        1993, pp.135-142.

[84]   X. Xia, P. Sakaris and H J. McQueen, "Hot Torsion Behaviour and

        Recrystallization of SiCp/6061 Al Composite", **Composite Materials(ICCM-9)**,

        Vol. 1, ed. A. Miravete, Madrid, Spain, 1993, pp 157-162

[85]   I. C. Smith, G. Avramovic-Cingara and H. J. McQueen, **Aluminum-Lithium Alloys**, eds. T. H. Sanders, et. Al., MCPE Pub., Birmingham, UK, 1989, pp.223-232.

[86]   H J. McQueen and N. Ryum, **Scand. J. Met.**, 14, 1985, pp.183-194.

[87]   B. Verlinden, P. Wouters and H. J. McQueen, **Mat. Sci. Eng.** A123, 1990, pp. 229-237 and 239-245

[88]   H. J McQueen and P. Sakaris, **Aluminum Alloys: Physical and Mechanical Properties**, vol. 2, ICAA 3, eds. L. Arnberg et al., NIH-Sinteff, Trondheim, Norway, 1992, pp.179-184.

[89]   C.Rossard and P.Blain, **Met.**, 55, 1958, p.573.

[90]   C.Rossard and P.Blain, **Met.**, 56, 1959, p.286.

[91]   M.J.Luton and C.M.Sellars, "Dynamic Recrystallization in Nickel and Nickel-Iron Alloys during High Temperature Deformation", **Acta. Metall.**, vol 17, 1969, pp.1033-1043.

[92]   S.Sakui, T.Sakai and K.Takeishi, **Trans.** ISIJ, 17, 1977, p.718.

[93]   T.Sakai, M.G.Akben and J.J.Jonas, "Thermomechanical Processing of Microalloyed Austenite", eds. A.J.DeArdo, G.A.Ratz and P.J.Wray, AIME, Warrendale, Pa., 1982, p.237.

[94]   H.J.McQueen and J.J.Jonas, "Recovery and Recrystallization during High Temperature Deformation", **Treatise on Materials Science and Technology**, vol. 6, ed R.J Arsenault, New York, Academic Press, 1975, pp.393-493.

[95]   R.A.Petkovic, M.J.Luton and J.J.Jonas, "Recovery and Recrystallization of Carbon Steel Between Intervals of Hot Working", **Canadian Metallurgical Quarterly,** vol. 14, No. 2, 1975, pp.137-145.

[96]   S.L.Semiatin, G.D.Lahoti and J.J.Jonas, "Mechanical Testing", 8, ASM **Metals Handbook,** 9th Edition, ASM, Metals Park, Ohio, 1985, p 154

APPENDIX

Furnace Programming

Furnace control is by 2 interconnected devices: the furnace controller (smaller device), resting on top of the setpoint programmer (larger device)

1 On the setpoint programmer, turn the key to PRGM position.

2 Press RESET PRGM, then 1 (i. e. output channel 1), then ENTER, then REGION, then ENTER (this clears the previous program).

3 Press LOAD PRGM, then 1, then ENTER

4 Press L RANGE, enter -18; then press H RANGE, enter 1371

5. Press REGION, enter 0; press SOAK AT, enter 0; press TIME, enter 0 hr 10 min.

(**NOTE**. although values are entered as "hr" and "min.", the program actually runs as "min." and "sec" using the '60X' feature.)

6 Press REGION, enter 1, press RAMP TO, enter the value; e.g. 300°C

Press TIME, enter the values; e.g. 5 min. and 00 sec.

7 Repeat Step 6 for each region of your temperature setpoint program.

8 Review the entered program by repeatedly pressing CLEAR until TEST PRGM flashes, then press TEST PRGM, wait for LED test to completed, enter 1, then go through each region of the program

9. Press CLEAR repeatedly until TEST PRGM flashes, then turn key to 60 X

Running the Furnace

1. Ensure that the cooling water is on.

2. On the furnace controller, press for closed loop control

(manual control is: ✍)

3. Ensure remote setpoint.

4. Ensure setpoint is zero by pressing RESET PRGM, then START on the

setpoint programmer, waiting a sec. or two for the setpoint to be

transmitted to the furnace controller, then pressing STOP.

5. Ensure power output is zero by monitoring OUTPUT (readout is in %)

6. Switch on the 460V power supply.

7. Ensure cooling water is on, then adjust the Argon flow so that bubbles appear

8. Press START on the setpoint programmer (remember that the first region --

REGION 0 is a 'soak' for 10 sec.

9. Suggestion: always monitor OUTPUT to make sure that all is OK

** If OUTPUT goes much above 50%, SWITCH OFF 460V SUPPLY **
(or else things may **MELT!**)

1. Sample program for isothermal continuous test.

Testing conditions: $T = 300°C$; $\varepsilon = 5.0$; and $\varepsilon = 1.0s^{-1}$.

Therefore time required for complete the testing = $\varepsilon/\dot{\varepsilon}$.

1. On the setpoint programmer, turn key to PRGM position.

2. Press RESET PRGM, then press 1, then ENTER, then REGION, then ENTER.

3 Press LOAD PRGM, then 1, then ENTER.

4. Press L RANGE, enter -18; then press H RANGE, enter 1371.

5. Press REGION, enter 0; Press SOAK AT, enter 0; then press TIME, enter 0 min. 20 sec.

6 Press REGION, enter 1, press RAMP TO, enter 300, press TIME, enter 5 min. 0 sec.

7. Press REGION, enter 2, press SOAK AT, enter 300, press TIME, enter 5 min. 0 sec.

8. Press REGION, enter 3, press SOAK AT, enter 300, press TIME, enter 0 min. 5 sec. (Time required for completing the testing)

9. Press CLEAR until TEST PRGM flashes for reviewing the entered program

10. Press TEST PRGM, wait for LED test to complete, then press 1; then go through each region of the program.

11. Press CLEAR repeatedly until TEST PRGM flashes, then turn key to 60X.

12 Running the furnace.